

JETS, MODELS VERSUS EXPERIMENTAL DATA I

FERMILAB-Conf-82/86

Risto Orava*

Fermi National Accelerator Laboratory
P.O. Box 500, Batavia, Illinois 60510

U.S.A.

Abstract

Present status of jet studies is reviewed with the special emphasis on the merits of various tests of jet models.

*R.R. Wilson Fellow at Fermilab; on leave of absence from the University of Helsinki, Helsinki, Finland.

CONTENTS:

Foreword

1. Introduction
Motivation
Models
Hadronization
Jets, Jets, Jets . . .
This talk
2. Parton Jets-Hadron Jets
Space-Time Evolution
Rapidity Distribution
Kinematical Range
Hierarchy of Models
Field and Feynman Jets
Longitudinal Phase Space
Limited P_T Jets
Angular Jets
Cluster Jets
Inclusive Jets
3. Detailed Properties of Quark Jets
Factorization
Local Quantum Number Compensation
Jet Charge and Low Energy Effects
SU(3) Symmetry Violation in Hadronic Vacuum
4. QCD Jets
Soft and Hard QCD Quanta
Space-Time Evolution Modified
Preconfinement
Field and Feynman Jets with Gluons
Strings Attached
Jet as a Branching Process
Recipes and Objections
A Test of Perturbative QCD
 Q^2 Evolution of e^+e^- x-distributions
5. Conclusions

Jets of hadrons should result from parton confinement. Thus, when studying strong interactions experimentally we have to deal with hadrons - the asymptotic states of the partons. It is the conventional wisdom about spacetime evolution of the partonic asymptopia that directs us to look for and to investigate kinematically distinct showers of hadrons - the jets.

The simplest, zeroth order picture of partons is shown to work in lower energy e^+e^- annihilation into hadrons and in deeply inelastic lepton production of hadrons. In the more involved multiparton interactions of hadron-hadron collisions no such immediate consistency with the naive picture exists. This failure to comply with a simple-minded scenario for hadron-hadron jet production has prompted some of us to throw our towels in the ring and shout: "I don't believe in jets!" Disregarding the fact that we are not dealing with a religion, this exclamation still is out of place. Not believing in jets is tantamount to not believing in partons. Such a heresy should lead to an easy conviction.

In my opinion, our primary task should not be to ask if there are some "jets" ad hoc but to ask how do the confined partons evolve to and manifest themselves as asymptotic hadronic states.

1. Introduction

MOTIVATION

QCD motivates and modifies the parton model description of hard scattering processes in which quarks and gluons appear both in the initial and final states. Quarks and gluons are not found unbound in the laboratory¹ but give - as bound states - a consistent picture of the observed hadron spectrum. - But how do these fundamental QCD quanta evolve into their asymptotic hadronic states, what is the mechanism that converts these color charged quanta into the color neutral particles? The only possible answer has to be given by similar experiments that, in the first place, proved that there are partons inside the observed hadrons².

The first attempt to organize and classify the multitude of data flowing from different hard scattering experiments is due to R.D. Field and R.P. Feynman³. Their parametrization of quark jet properties is still favored by a great majority of experimenters and phenomenologists. Although conceptually wrong⁴, their model has provided a wealth of information for data analysis. The Field and Feynman (FF) model has, in fact, found its way into analyses of every major hard scattering experiment of the 1980's.

A second generation model to probe parton final states is based on the Leading Logarithm Approximation (LLA) of perturbative QCD^{5,6,7}. In its inclusive (analytic) form, i.e. in the Jet Calculus of Konishi, Ukawa and Veneziano (KUV)⁸, inclusive particle distributions can be calculated for hard scattering processes and in an "exclusive" Monte Carlo version of QCD any hard scattering process can be studied in detail.

Within perturbative QCD one can define special variables in calculations that are free of singularities. These variables are chosen to be insensitive to the details of the hadronization process but they do serve to measure details of the hadronic final states produced in hard scattering⁹.

HADRONIZATION

The picture of parton final states in hard scattering processes has changed in the last five years but our perception of parton hadronization has not advanced simultaneously. To handle the kinematics more precisely and to account for the additional color degree of freedom, scenarios that are based on strings have been introduced^{10,11}. An ambitious "phase space" hadronizer has also been proposed by R.D. Field and S. Wolfram¹². Different input parameters in the parton "fragmentation" models have been extensively discussed, as well.

During the intense developments in theory, the experimentalist - looking for jets of hadrons - finds himself confused and lured by the theorist who designs predictions for the fictional jets of partons within a multitude of incomplete "QCD models" - 4-jets or others - that should possess a degree of predictive power. Only too often a comparison of the data - corrected for experimental uncertainties - proves inconclusive with respect to the model it is supposed to be testing. As a result a sincere and straightforward experimentalist directs his attention to more rewarding (?) problems like ν -oscillations or proton decay. Still the fundamental problem of strong interaction - confinement - is not understood.

THIS TALK

In this talk I shall make a clear distinction between the parton jets the theory tells about, and the hadron "jets" the experiments define. In Part I I will start by describing the theorists' and model builders' parton jets (Ch. 2) and the different kinds of jets the experimentalists define by the very setups of their experiments. I will proceed by discussing observables that serve as measures of detailed jet structures (Ch. 3). In Chapter 4 I will describe how QCD changes our space-time picture of parton final states and how the models parametrize the non-perturbative transition regions. In Part II I will concentrate on the production and properties of heavy quark jets, on baryons in jets and on the determination of the gluon fragmentation function. In my talk, I shall emphasize the relative merits of various models and the problems connected with the comparison of experimental data with the theoretical models. This concerns especially the different definitions of jets with which one has to deal in experiments and theory.

2. Parton Jets - Hadron Jets

SPACE-TIME EVOLUTION

Parton model jets are postulated to consist of hadrons with sharply cutoff transverse momenta relative to the initial parton direction³. Parton model jets are therefore "jetlike" by definition. The longitudinal structure of the parton model jets can be deduced by carefully studying the space-time evolution of the parton interaction. A general scenario for the

space-time evolution of parton final states was first brought up by J.D. Bjorken¹³ and it resulted in the so called "inside-outside" cascade models for parton hadronization.

In a parton final state, resulting from deeply inelastic lepton-nucleon scattering, for example, a quark and a di-quark are moving apart from each other at the speed $\sim c$. If we neglect the quantum fluctuations in the hadronic vacuum, the hadron production occurs on the hyperboloid defined by the hadron dimension of ~ 1 fm: $t^2 - x^2 = (1 \text{ fm})^2$ (Fig. 1)¹³. The hyperboloid joins the quark at $t = \gamma(1 \text{ fm})$ and, therefore, the overall timescale of the hadronization process is defined by the c.m.s. energy of the parton collision; $t \propto \sqrt{s}$.

Examples of hard scattering processes that factorize to the short time scale ($\tau \propto 1/\sqrt{Q^2}$) hard collision and to the long time scale ($t \propto \sqrt{s}$) hadronization process are shown in Fig. 2. The large difference in time scales t and τ at large Q^2 and not too small \sqrt{s} should ensure factorization of the two processes and should motivate the expectation that jets are universal to all hard scattering processes. By introducing probabilities $P_i(x)$ for finding a quark of flavor i and momentum fraction x , and by defining fragmentation functions $D_i^h(z)$ for the quark i , the factorization hypothesis can be expressed as

$$\frac{d\sigma}{dz} = \sum_i p_i D_i^h(z) \quad (1)$$

Table 1 gives probabilities p_i for four different hard scattering processes defined in Figures 2. In the inside-outside cascade models, like in the one by S. Brodsky and N. Weiss¹⁴, the final state hadrons are at spacelike separation and the creation of one hadron cannot cause the emission of another hadron. Short range particle-particle correlations dominate. In these models the trigger for particle emission must come from the region where $t^2 - x^2 < (1 \text{ fm})^2$. In the model of Brodsky and Weiss this is accomplished by emitting a large number of gluons at $x=t=0$ with a flat distribution in rapidity. In the model the gluons are assumed to live, on the average, a constant characteristic proper time $t \sim 1 \text{ fm}^{-1}$ and then produce a $q\bar{q}$ -pair. The production of $q\bar{q}$ -pairs thus happens next to the hyperboloid $t^2 - x^2 = (1 \text{ fm})^2$. Hadrons would then be created by joining quarks and antiquarks from adjacent gluons into color singlets. The model leads to the local compensation of quantum numbers and it has short range correlations in rapidity.

RAPIDITY DISTRIBUTIONS

The rapidity distributions expected for hadrons created in the inside-outside cascade scheme are shown in Fig. 3 for the three hard scattering processes. In the simplest case of e^+e^- annihilation to hadrons, a plateau of "central" hadrons separates the quark and antiquark fragmentation regions (Fig. 3a). In lepton scattering additional structures from the target fragments - the spectator quarks - and from the hole left behind by the struck quark are present¹³ (Fig. 3b). At sufficiently high energies an insulating plateau of hadrons, moving slowly with respect to the c.m.s, is present between the different fragmentation regions. For high P_T hadron-hadron scattering the situation should be significantly more complex. Depending on the fractional energies of the partons participating in the hard scattering process, different rapidity distributions should result. It would be hard to envision a situation where a clear separation between the jets existed when averaged over many events (Fig. 3c).

KINEMATICAL RANGE

Kinematical range in the e^+e^- experiments is uniquely defined by the c.m.s. energy \sqrt{s} that also defines the "offshellness" of the created $q\bar{q}$ pairs (Q^2). In lepton-nucleon scattering the kinematical range of any given hadronic final state depends on the c.m.s energy $W=\sqrt{s}$ and on $Q^2 = -(l-l')^2$ (\vec{Q} defines the direction of the struck quark). The total rapidity range is proportional to $\log W^2$, whereas the current fragmentation region extends a length proportional to $\log Q^2$. In the "deeply inelastic" hadron-hadron collisions one has to fold in the parton fractional momentum distributions both in the projectile and target hadrons to be able to calculate the kinematical ranges for the hard scattering processes. For any single event neither the struck parton direction nor its momentum are known. Using the parton momentum density distributions measured in deeply inelastic lepton-nucleon scattering we can estimate the average energy in a hard scattering process of a hadron-hadron interaction: we find that in a quark-quark collision of a proton-proton interaction there is available about 10% of the total proton-proton c.m.s energy, i.e. $\sqrt{s_{qq}} \approx .10 \sqrt{s_{tot}}^{15}$. For πp collisions the available energy is $\sqrt{s_{qq}} \approx .15 \sqrt{s_{tot}}^{15}$.

HIERARCHY OF MODELS

To parametrize the transition of partons into hadrons (Fig. 1) a model is required. Here two basically different approaches have been introduced. In the Field & Feynman Jets the parton model or a perturbative QCD calculation is employed to obtain a weight for a particular parton final state that is subsequently transformed into hadrons in a typical mass scale of about 4 GeV by using a phenomenological parametrization. In the second approach - that is supposedly valid at very high energy - the parton evolution is treated by employing leading logarithm approximation of the perturbative QCD down to relatively small invariant masses where different prescriptions are applied for the transition of partons into hadrons. In Table 2 hierarchy of these hadronization models is described. Baryon production, heavy quark fragmentation and a detailed diquark fragmentation model have been added to some of these models. The KUV jet calculus has recently been employed to produce partons at different fractional momenta that are subsequently recombined into hadrons using specific recombination functions from soft hadron-hadron processes¹⁶.

Several supplementary models¹⁷ have also been introduced (Part II) and can be combined with the basic models to treat the details of parton hadronization in more detail.

FIELD and FEYNMAN JETS

The first systematic framework to classify the hard scattering data on jet production is due to R.D. Field and R.P. Feynman³. In the FF model the quark jet properties are parameterized in terms of a "momentum sharing function" $f(\eta)$, $f(\eta)=1-a+3a\eta^d$ ($a=.77$, $d=2$. give an acceptable fit to the low energy data) which describes the probability that the primary meson (contains the original quark) leaves a fraction η of the quark momentum to the rest of the quark jet cascade. The recursive scheme for the meson distribution in a quark jet cascade is then expressed by the integral equation

$$D_q^h(z) = f(1-z) + \int_z^1 \frac{d\eta}{\eta} f(\eta) D_q^h\left(\frac{z}{\eta}\right), \quad (2)$$

where the function $D_q^h(z)$ is known as the quark q "fragmentation function" to hadron h.

Besides function $f(\eta)$ the FF model requires the following parameters:

- (i) Relative suppression of strange quark-antiquark pairs in the quark jet cascade ($\lambda=0.5$).
- (ii) Spin nature of the primary mesons. (Only pseudoscalars and vectors are considered with $\alpha_{ps} = \alpha_v = 0.5$.)
- (iii) The mean transverse momentum allocated to the primary mesons (σ^2 in the Gaussian $d\sigma/dP_T^2 \propto \exp(-\langle P_T^2 \rangle / \sigma^2)$ with $\sigma=330$ MeV).
- (iv) Baryon production is not considered in the model; an extension that includes baryon production requires further parameters¹⁷.
- (v) The recursive generation of new particles continues until a cutoff momentum ($P_0=330$ MeV).

The FF model thus contains at least eight (8) parameters whose energy dependence is poorly known. We shall later discuss these parameters in detail.

In reference to our discussion of the space-time evolution of the parton final states, there are defects in the FF jet parameterization scheme:

- (i) The space-time evolution of the FF jet is "outside-in", i.e. the primary hadrons are generated first.
- (ii) The energy is not strictly conserved.
- (iii) The transverse momentum cutoff is artificial and dilutes any predictive power one might have regarding the transverse structure of jets.

The FF jet generation algorithm is presented below in terms of a flow diagram.

Field & Feynman Jet Algorithm

Initial quark with momentum
 W_0

Generate fractional momentum
 $\eta = 1-z$ randomly with
 $f(\eta) = 1 - a + 3a\eta^2$

Generate pairs $u\bar{u}, d\bar{d}, s\bar{s}$ with
probabilities γ, γ or $\gamma_s = 1 - \gamma_s$

Decide spin-parity
 $\alpha_{ps} = \alpha_v = 0.5$

$W_0 = \eta W$
 $q = u, d$ or s

$W_0 > P_0 = 300$ MeV?

NO

Add k_T with

$\exp(-q_{T1}^2 / 2\sigma^2) dq_T^2$

Let vector particles
and η, η' decay
FF Jets

In Fig. 4 FF parameterization of various hard scattering data on $D_q^{h\pm}(z)$ functions are shown. The only change from the original FF parameters is an adjustment of λ from 0.5 to 0.27 as measured in an antineutrino experiment at Fermilab¹⁸. All measurements are well parametrized by the FF algorithm despite of the conceptual problems with the model. Therefore, a model that incorporates a rapidity plateau, short range correlations and an adequate treatment of resonances seems to be enough to describe longitudinal jet properties at Fermilab energies.

LONGITUDINAL PHASE SPACE

A popular way to compare predictions or parameterizations of dynamical models to the experimental observations is to use so called Longitudinal Phase Space Models (LPS) which supposedly represent "uncorrelated" schemes for particle production. The calculation usually begins by generating the available energy for the "event". This is done with varying input assumptions, and they usually include the basic folklore about the parton distributions in the nucleons and certainly consistency with the standard model. Observed distributions of inelasticity are used in lepton interactions, for example. The required details of an individual event depend on the apparatus used in the experiment, but usually the following steps are taken¹⁹:

Generate initial parton
energies from measured
parton distributions
 $xq(x)$, $xg(x)$

Generate $-q^2$ for an event

Generate recoil nucleon
for lepton interaction
with a flat x distribution.
This gives the available
energy for hadron production.

Choose particle multiplicities
using isospin symmetry
 $(\langle \pi^+ \rangle + \langle \pi^- \rangle) / 2 = \langle \pi^0 \rangle$ and
Poisson distributions for $\pi^- \pi^0$.
Energy conservation can be used
to get number of π^+ 's.
For energy dependence of $\langle n \rangle$
experimental data is used.
Ratio K/π is obtained
from experimental data.

Choose P_T according to
 $d\sigma/dp_T \propto \exp(-6m_T)$
and assume
flat azimuthal angle
distributions,

Demand p_T to be conserved.

Calculate $P_{||}$ in the s
rest frame.

Flat Y , with $\Delta Y = 2 \ln \sqrt{s} - 0.4 \ln m_T$
 $P_{||} = m_T \sinh Y$

Demand $P_{||}$, E to be conserved

Transform hadrons back to
the laboratory system

"UNCORRELATED" LPS EVENTS

At relatively low effective energies ($\sqrt{s} \leq 10$ GeV) hadron production can be described by the LPS models. The message from this agreement is not straightforward, however. The limited $P_T (\propto \exp(-6m_T))$ is an experimental observation and an inherent assumption for the parton model jets. The basic parton model kinematics is also assumed by the use of the observed parton momentum density distributions and the observed charge correlations are imposed in an average sense by using the measured average multiplicities.

In Fig. 5 data on fragmentation functions $D_q^h(z)$ are shown with a LPS prediction²⁰. From the agreement of the LPS prediction with the data we conclude that the longitudinal structure of a quark jet is not very sensitive to the detailed dynamics of the hadronization process at low energies ($\sqrt{s} \leq 10$ GeV). Due to the implicit charge correlations in the model it is hard to draw any further conclusions from this agreement. In fact, a more detailed analysis shows that not all quark jet properties at low

energies ($\sqrt{s} \leq 10$ GeV) are reproduced by the LPS models. The fastest-second fastest particle correlations measured in a quark jet favor the FF jet model over the LPS scheme²⁰. Also, the net electric charge distribution in rapidity is not reproduced by the LPS model²²¹.

LIMITED P_T JETS.

It was originally conjectured - in guidance from the experimental data - that in a quark jet the average momentum transverse to the jet axis was fixed at around 360 MeV/c. The sharp cutoff in P_T serves as the basis for visualization of a jet as spray of hadrons each contained in a cylinder with a radius of about 360 MeV/c (Fig. 6). The "jettiness" of a collection of observed hadrons would then be pronounced if the (limited) P_T would be small compared to the longitudinal extension of the momentum cylinder, i.e. if $\langle P_T \rangle \ll P_{\text{quark}}$.

ANGULAR JETS

A Limited P_T Jet becomes the Angular Jet (Fig. 7) if we assume that the ~~distribution of the longitudinal~~ momentum fraction $z = P_{\parallel} / P_q$ carried by a hadron in the limited P_T jet is independent of the parton momentum P_q (Scaling). The hadrons with the (limited) P_T of $\langle P_T \rangle$ would then appear in a cone with an opening angle $\langle \delta \rangle$

$$\langle \delta \rangle \approx \langle P_T \rangle / \langle z \rangle P_q \approx \frac{\langle P_T \rangle \langle n \rangle}{2 P_q} \quad (3)$$

The Angular Jets would then become more and more collimated with increasing P_q ; for $P_q = 6.5$ GeV we get $\langle \delta \rangle \approx 27^\circ$ whereas for $P_q = 15$ GeV we find $\langle \delta \rangle \approx 12^\circ$.

An analysis based on the FF quark Jets ($e^+e^- \rightarrow q\bar{q} \rightarrow \text{hadrons}$) shows that the angle between the two most collinear particles in an event has a relatively wide distribution that peaks at about 10° independently of energy (Fig. 8)²². An angular cone of about 30° would contain most of the particles in a jet. The long tail of the angular distribution implies that many of the less collinear particles would not be counted into the Angular Jet even in this idealized example.

The z-distribution softens at higher energies and with $\sqrt{s}=30$ GeV the average angle will be larger: $\langle\delta\rangle \approx 18^\circ$ instead of 12° as calculated by assuming the scaling z-distribution ($\langle z \rangle = .20 + .13$)

CLUSTER JETS

Recently a number of cluster algorithms have been devised to identify jet structures in multihadron final states²². Usual methods of jet analysis (thrust, sphericity, triplicity,...) fix the number of jets a priori and thereby impose kinematical constraints for the final states: collinearity for the 2-jet events and planarity for the 3-jet events. Cluster algorithms should avoid these problems.

A typical cluster algorithm consists of two steps: (1) Definition of "preclusters" of particle pairs having their momentum vectors within a predetermined angle α and (2) merging of the preclusters into "clusters" having their momentum vectors within a predetermined angle of β . To identify a cluster with a "jet" one demands a minimum cluster energy of 2 GeV. From an experimental analysis it is found that the maximum efficiency for the cluster algorithm is achieved with about 30° "collecting angles" α and β . Note that 30° collecting angle corresponds to about 7% of the full 4π solid angle. The cluster algorithm gives, besides the number of "jets" (N_j) in an event also the energy and momentum of the jet.

Recent results from a test of a cluster algorithm are shown in Fig. 9 in which the number of "jets" found using the cluster algorithm in $e^+e^- \rightarrow$ hadrons is compared with the Monte Carlo expectations for $e^+e^- \rightarrow q\bar{q} \rightarrow$ hadrons and for $e^+e^- \rightarrow q\bar{q}G \rightarrow$ hadrons²². The fact that the data points lie between the Monte Carlo expectations supports the use of this cluster finding algorithm in jet analysis.

The cluster analysis is based on the intuition of the Angular Jet i.e. on the following two assumptions (1) limited P_T and (2) scaling of the fractional energy distributions of hadrons in the jet. In the Angular Jet it is the particle direction and its angle with the neighboring particle that establishes the jet membership. For an occasional offspring with a large angle or with intrinsic softness the membership is not guaranteed. In an average sense the Cluster Jet provides an alternative jet definition that constraints less the kinematics of the final state.

A Cluster Jet Algorithm ²²

Define momenta, \vec{P}_i , direction, $\vec{n}_i = \vec{P}_i / |\vec{P}_i|$, and energy, E_i , for every particle i in the final state.

Define "preclusters" D_i :

- each particle i is a member of only one precluster D
- any two particles i, k belong to the same precluster if $\vec{n}_i \cdot \vec{n}_k > \cos \alpha$ for a predefined α .

Define "clusters" C_i :

- each precluster D_i is a member of only one cluster C
- any two preclusters D_i, D_k belong to the same cluster if $\vec{n}_{D_i} \cdot \vec{n}_{D_k} > \cos \beta$ for a predefined β .

Define "Cluster Jet", J_i :

- to be accepted as Cluster Jet J_i a cluster C_i has to:
 - (1) belong to the minimal set of clusters n_c ; $n_c = \sum_{i=1}^{n_c} E_{C_i} > E_{tot}(1-\epsilon)$ for a predefined value of ϵ ; E_{tot} is the sum of particle energies and the cluster energy E_{C_i} is given as

$$E_{C_i} = \sum_{k \in C_i} E_k$$

- (2) $E_{C_i} > E_{th}$ for a predefined threshold energy E_{th}

Set of Cluster Jets

INCLUSIVE JETS

The Limited P_T Jets, Angular Jets or Cluster Jets do not provide us with a jet definition that could be employed in a detailed analysis of jet properties. Each definition corresponds to a special feature of a

collection of hadrons that are supposed to result from parton hadronization. The Field-Feynman Jets give us some insight in the longitudinal structure of quark fragmentation. The Uncorrelated LPS Jets indicate that it is the short range correlations and the right mass scale of few hundreds of MeV's (in addition to the conservation laws) that really matter in getting this insight.

To study parton transformation into hadrons an inclusive jet definition is required. To define the Inclusive Jets the rapidity distribution of hadrons resulting from a hard scattering process has to be considered. At sufficiently high energy a simple cutoff in rapidity ensures a proper definition of the the parton jet in the e^+e^- annihilation to hadrons or in the lepton-nucleon collisions.

3. Detailed properties of quark jets.

FACTORIZATION

Experimentally the factorization hypothesis (Eq. 1) is valid within 20%. In Fig. 10 $\bar{\nu}N$ data on $R=D(z_1, x_1)/D(z_1, x_2)$ are plotted for different (fixed) Q_0^2 (Ref. 21). Within experimental accuracy the x, z factorization works. In Fig. 11 recent data from the European Muon Collaboration (EMC) are plotted for $D(x_1, z_1, Q^2)^{23}$. Although some indications for factorization breaking are observed at the edges of available phase space we do conclude that the factorization hypothesis remains approximately valid.

LOCAL QUANTUM NUMBER COMPENSATION

An effective way of testing the cascade picture of parton hadronization is to check how locally the quark quantum numbers are compensated in the rapidity space²⁴. Purely statistical charge distribution in the final state would result, as we shall see, in about one unit of rapidity for the average compensation length of the electric charge. Local Charge Compensation (LCC) would then lead to a compensation length that is significantly smaller than one unit of rapidity. In Fig. 13 the rapidity zone lengths are plotted for $\bar{\nu}N$ charged current interactions in the deeply inelastic region^{25,26}. Definition of the zone length distribution $Z(y^*)$ is given in Fig. 12 and can be formulated in terms of the step function $\theta(y^*-y_1^*)$ as

$$Z(y^*) = \sum_i e_i \theta(y^* - y_i^*). \quad (4)$$

To check how much influence the ambiguous definition of the current fragmentation region²⁵ has in the zone length distributions we have used two alternative definitions of the rapidity zones. In the first definition only zones fully within the forward c.m.s. hemisphere (in the current direction) are accepted and in the second one a zone overlapping with the backward c.m.s. hemisphere is allowed. For a more complete analysis a sample of νH_2 interactions would be required. With our method we see, nevertheless, that there is a significant difference in the zone length distributions in these two cases (Fig. 13). Strictly forward zones are shorter, on the average, than the ones with one overlapping zone. In Fig. 14 we show the average rapidity zone length $\langle \lambda \rangle$ as a function of the c.m.s. energy for the two definitions. For comparison we have also included data from pp experiments²⁶. The dashed line represents a result obtained by randomly reassigning the electric charges of the hadrons in the νN final states.

As a conclusion we note that while the electric charge is locally compensated in quark hadronization (forward zones) the test of the LCC hypothesis is effected by the relatively low available energies, i.e. the overlap between the current and target fragmentation regions.

JET CHARGE AND LOW ENERGY EFFECTS

It is well known by now that the rapidity plateau is not a good insulator of the additive quark quantum numbers in the quark fragmentation region but the plateau acts more like a dielectric²⁷. Quark quantum numbers leak through the plateau: we find in the simple incoherent parton model picture that the average jet charge $\langle Q_{jet} \rangle$ is given as

$$\begin{aligned} \langle Q_{jet} \rangle &= e_q - \langle e_q \rangle \\ &= e_q - \sum_i \gamma_i e_i \\ &= \begin{cases} 1 - \gamma_u & \text{for a u-quark jet} \\ -\gamma_u & \text{for a d-(s-) quark jet} \end{cases} \end{aligned} \quad (5)$$

Here e_q is the electric charge of the quark q and γ_i the probability of forming a quark-antiquark pair of flavor i in the quark jet cascade.

Hence, by measuring the (clean) jet charge one actually measures the probability γ , not the quark charge²²⁸. One may extend this discussion to other additive quark quantum numbers, and for jet strangeness one obtains, for example:

$$\begin{aligned} \langle S \rangle &= S_q - \langle S_q \rangle \\ &= \gamma_s, \end{aligned} \quad (6)$$

i.e. $\langle S \rangle$ is proportional to the probability of forming a $s\bar{s}$ pair in the hadronic vacuum.

There is a severe problem in the experimental analysis of jet quantum numbers : At finite energies one never observes the pure quark jet but there exists an overlap in phase space between the hadronization products (hadrons) of the quark and the spectator quark system. At low energies ($W < 10$ GeV) there is not enough phase space for sufficiently clean jets to be observed. We have earlier shown that this overlap in rapidity can be well parameterized using the form W^{-1} or, equivalently, $Q^2(1-x)^{-1/2}$ (Fig. 15). One should note that with fixed large x this effect prevails at large Q^2 and introduces a new mass scale relevant in defining the kinematical domain where perturbative QCD could be tested. Experimental measurements that utilize the charge extrapolation give $\gamma = .44 \pm .09$ (Ref. 28).

SU(3) SYMMETRY VIOLATION IN HADRONIC VACUUM

If we consider three quark flavors only, we may simply connect the probabilities γ_1 and relative suppression of strange quarks, $\lambda = \gamma_u/\gamma_s \approx \gamma_d/\gamma_s$. From probability conservation ($\gamma_u + \gamma_d + \gamma_s = 1$) we get γ in terms of the jet charge as

$$\begin{aligned} \gamma &= \frac{2\langle Q \rangle - 1}{1 - \langle Q \rangle} \quad \text{for a u-quark jet} \\ &= - \frac{1 + 2\langle Q \rangle}{\langle Q \rangle} \quad \text{for a d-(s-) quark jet} \end{aligned} \quad (7)$$

Unfortunately, the $(\nu)N$ measurements are not accurate enough to set any significant constraints on λ . There is, however, a better measurement in an $e(\mu)N$ experiment²⁹.

Our prediction should now account for the mixture of quark flavors involved in the electromagnetic coupling (see Eq. 1, p. 5) and it results in the formula:

$$\lambda = \frac{1-2 (8/9 - \langle Q_{jet} \rangle)}{8/9 - \langle Q_{jet} \rangle} \quad (8)$$

with the measured value of $\langle Q \rangle = .44 \pm .01$ we obtain for λ : $\lambda = .23 \pm .05$.

In $\nu_{\mu}N$ interactions we can measure λ directly as the ratio K^0/π^- (at the limit $z \rightarrow 1$) between the inclusive production rates of K^0 's and π^- 's in the current fragmentation region^{2,18}. Our result $\lambda = 0.27 \pm 0.04$ is well consistent with the previous eN result derived from the jet charge measurement.

We have recently combined a variety of results for λ and find a good consistency between results from different reactions and from different methods¹⁵. Within the experimental accuracy λ stays constant as a function of available energy between 1 and 34 GeV (Fig. 16).

4. QCD JETS

SOFT AND HARD QCD QUANTA

QCD modifies the parton model jets in two qualitatively different ways: (i) By emission of soft gluons with the mass spectrum dt/t , and (ii) by emission of hard gluons that carry a finite fraction of the available energy. While the probability for emitting a soft gluon at the limit $t \rightarrow 0$ is infinite, the probability of emitting a hard gluon with angle θ with respect to the direction of the momentum of the charge moving with velocity $u \sim c$, is

$$\frac{dP(\theta)}{d\Omega/2\pi} \approx \frac{\alpha_s}{\pi} \frac{\sin^2\theta}{(1-u \cos\theta)^2} \quad (9)$$

where α_s is the strong coupling constant. The hard gluons will thus be mostly emitted into a narrow angular cone with half opening angle of $\theta \sim 1-u^2 \sim E_q/\mu_q$, where E_q and μ_q are the energy and "mass" of the parent quark. The overall probability for the hard gluon emission is then

$$P \approx \frac{\alpha_s}{\pi} \ln(E_q^2/\mu_q^2) \quad (10)$$

For $E_q \sim 10$ GeV we find for P , $P \sim 0(1)$. QCD thus "dresses" up the parton model jets by a multitude of soft ($t \rightarrow 0$) gluons and by a limited number of hard, mostly collinear gluons.

SPACE-TIME EVOLUTION MODIFIED

The off-shell mass of a quark defines its lifetime before the emission of a gluon: For a fast moving quark with energy $E_q = \sqrt{s}/2$ the lifetime τ is $\tau \sim (E/q^2)(1/q^2) = E/q^2$. With the notation of Fig. 17 we find

$$\begin{aligned} q^2 &\approx 2kk_1 = 2 \frac{E}{2} (1-z) \frac{E}{2} z(1-\cos\theta) \\ &= E^2 z (1-z) \sin^2 \frac{\theta}{2} \end{aligned} \quad (11)$$

i.e.

$$\tau = 1/ E(z(1-z)\sin^2\frac{\theta}{2}) \quad (12)$$

Therefore, the time scale involved in gluon emission is small if $\sqrt{s} \gg 1$ GeV.

We may compare the timescale for gluon emission (Eq. 12) with the hadronization time scale of page 5, i.e. with $t = \sqrt{s}/\mu$ and conclude that to emit a gluon before the complete screening of color charges (by new $q\bar{q}$ pairs from hadronic vacuum) the condition

$$E^2 z(1-z)\sin^2\frac{\theta}{2} > \mu^2 \quad (13)$$

or

$$k^2 > \mu^2 \quad (14)$$

must be fulfilled (see Fig. 18). With multiparton final states the

off-shell masses of all partons will decrease sharply with further branching processes and condition (14) should be all that is required for gluon emission to occur before the hadronization takes place. Due to confinement, the probability of the created partonic final states to turn into hadronic final states has to be equal to one. How this transition takes place QCD can presently say nothing about and different models are used to parametrize the transition regions in Fig. 18.

PRECONFINEMENT

Description of the evolution of a jet in space and time is not sufficient in QCD with its colored quanta: One also has to understand how the color degree of freedom evolves into the asymptotic color singlet hadrons. It has been recently argued by Amati and Veneziano³⁰ that, in what they call "preconfinement", quarks and gluons produced in the jet evolution from mass of k^2 down to the "preconfinement mass" of μ^2 , become organized in clusters of color singlets with finite, k^2 - independent masses of order μ . It is then left to the soft confinement to turn these color singlets of mass $\sim O(\mu)$ into hadrons. Preconfinement would then act as a color neutralizer at the end of the parton jet evolution. We should emphasize here the importance of soft hadronization; were there some hard color reshufflings taking place at this stage, the jet properties might be drastically altered (see p. 5). In the space-time picture the transition region of Fig. 1 would now be completely "evaporated" (Fig. 19).

FIELD & FEYNMAN JETS WITH GLUONS

The most straightforward way to incorporate perturbative QCD effects in the Field & Feynman jets is to write the cross section for e^+e^- annihilation as the sum of two pieces³¹ i.e.

$$\sigma_{\text{jet}} = \sigma_{q\bar{q}} + \sigma_{q\bar{q}G} = \left(1 + \frac{\alpha_s}{\pi}\right) \sigma_0, \quad (15)$$

where $\sigma_{q\bar{q}}$ stands for the two-jet cross section, $\sigma_{q\bar{q}G}$ for the 3-jet cross section, σ_0 for the parton model prediction and α_s is the running coupling constant of QCD. The three-jet cross section $\sigma_{q\bar{q}G}$ is given as

$$\frac{1}{\sigma_0} \frac{d\sigma(q\bar{q}G)}{dx_q dx_{\bar{q}}} = \frac{2}{3} \frac{\alpha_s(Q^2)}{\pi} \frac{x_q^2 + x_{\bar{q}}^2}{(1-x_q)(1-x_{\bar{q}})} \quad (16)$$

in terms of the fractional energies of the quark and the antiquark. The two-jet rate may then be expressed as

$$\sigma_{q\bar{q}} = \sigma_0 - \left(\sigma_{q\bar{q}G} - \frac{\alpha_s}{\pi} \sigma_0 \right) \quad (17)$$

and the Field & Feynman jet algorithm may be used for hadronization of this class of events. The rate of three-jet events is ambiguous due to the divergent cross section (Eq.16) at $x_q, x_{\bar{q}} = 1$ or at $\theta=0$ or $\theta=180^\circ$ (Eq. 9, page 18). A cutoff in the matrix element (Eq. 16) is required. In the model of Hoyer et al.³¹ the cutoff procedure is simple and well defined; there three-jet rate is obtained as

$$\sigma_{q\bar{q}G} = \int_{2/3}^{T_0} dT \frac{d\sigma_{q\bar{q}G}}{dT} \quad (18)$$

where the cutoff value for thrust, T, is defined by

$$\frac{d}{dT} \left(\frac{d\sigma(q\bar{q})}{dT} \right)_{T=T_0} = 0 \quad (19)$$

with T_0 varying as a function of the c.m.s. energy. The cutoff varies from $T_0=.92$ to $.98$ for $Q=15$ to 90 GeV. The three-jet fraction varies correspondingly from $\sigma_{3jet}/\sigma_0 = .17$ to $.49$. For the three-jet event class one may use the Field & Feynman jet algorithm with a special treatment of the hard gluon; in the model of Hoyer et al. the gluon is treated as a $q\bar{q}$ -system with flavors u,d or s coming in ratios of 2:2:1.

The warnings the authors of the Hoyer model issue are the following:

1. The model should not be used at higher energies ($Q \geq 90$ GeV) because the probability conservation is enforced by

$$\sigma_{2-jet} + \sigma_{3-jet} = \left(1 + \frac{\alpha_s}{\pi} \right) \sigma_0 \quad (20)$$

that cannot possibly work once $\sigma_{3-jet} > \sigma_0$.

2. Little is known about the higher order corrections of QCD that are likely to introduce significant contributions beyond the $O(\alpha_s)$

perturbative QCD calculations.

3. The 3-jet/2-jet separation is somewhat arbitrary and could lead to an ambiguity.

STRINGS ATTACHED

Jets never appear alone and the color field lines should always be attached into something else once a parton is pulled apart from its companions. Color carrying strings provide us with a useful way of following the color quantum numbers and other conservation laws through the hard process. Strings should also ensure a smooth transition from three-jet to two-jet events. The transition from a qqg event to a qq event could be defined in terms of the string mass M_s as the limit $M_s \rightarrow 0$ (Fig. 20). A gluon in the string model would consist of the two pieces of string sharing the gluon momentum; in the Lund model¹⁰ the gluon transforms into hadrons by first emitting a meson created around the "kink" where the two string pieces are connected together. The leftover strings hadronize independently in their rest frames. Glueball emission is not considered in the model. The hadronization of the strings is accomplished by a recursive technique resembling, in the end, the Field and Feynman jet algorithm. In one dimension the Lund model reduces to the Field & Feynman Jet picture¹⁰. In an extension to three dimensions a suppression factor from transverse motion effects arises in the "tunneling probability" of new qq pairs in the chromomagnetic field:

$$P = | (kd_{\perp}/m_{\perp}q_{\perp}) |^2, \quad (21)$$

where k is the string force constant, m_{\perp} the transverse mass of the quark-antiquark pair and d_{\perp} is the distance to be tunneled by the qq-pairs. In the Lund model a form

$$\begin{aligned} P(\alpha) &= |g(\alpha)|^2 = \alpha^2(\alpha^2 + 1)^{-1} \\ &= \Gamma/(\Gamma + m_q^2) \end{aligned} \quad (22)$$

is chosen for the probability P and a recursive scheme in which $\Gamma_0=0$ and

$$\Gamma_1 = (1-Z_{+1})(\Gamma_{(1-1)} + \frac{m_{\perp}^2}{Z_{+1}}) \quad (23)$$

is used for the quantities Γ_i . Here $m_{\perp i}$ is the transverse mass of a meson ($q_{i-1}\bar{q}_i$). Transverse momentum is generated according to a Gaussian $e^{-m_{\perp}^2/\sigma^2}$.

Perturbative QCD effects in the e^+e^- annihilation to hadrons are incorporated as in the previous model, i.e. $\sigma_{q\bar{q}} + \sigma_{q\bar{q}G} = (1 + \frac{\alpha_s}{\pi})\sigma_0$, but a more complex cutoff procedure is adopted in the Lund model than in the model of Hoyer et al. Referring to Fig. 20 the following selections are made:

1. Energy that is available for the string fragmentation is given as

$$M_{qG/2}^2 = (P_q + \frac{1}{2} P_G)^2 \quad (24)$$

If no string breakings occurs, i.e. if no new $q\bar{q}$ pairs are created the resulting final state is a $q\bar{q}$ -state. Also, if only one $q\bar{q}$ -pair is formed out of a string, the event is still chosen to be a 2-jet event.

2. If two or more string breakings occur, i.e. if two or more mesons are formed from one string the final state is classified as a $q\bar{q}G$ state.

A cutoff in the matrix element (Eq. 16) is also needed and it is obtained by considering "an average relative motion" of the newly created mesons. The cutoff in the string mass is then given as

$$M_{qG/2} \geq m_q + \frac{5}{2} m_a \quad (25)$$

where m_a is an "average meson mass" of about 700 MeV. A "suitable" cut is then deduced to be

$$x_2 < 1 - \frac{5m_a (5m_a + 4m_q)}{2E_{cm}^2} \quad , \quad (26)$$

with

$$M_{qG/2}^2 = m_q^2 + \frac{1}{2} E_{cm}^2 (1-x_2) \quad . \quad (27)$$

For x_1 a similar cutoff is applied. Moreover, a "weak gluon" cut is imposed by the condition

$$E_3^2 \geq 4 \text{ GeV}^2 \approx 8m_a^2, \quad (28)$$

since "the gluon loses energy twice as fast as a quark". In the c.m.s. E_3 is given as

$$E_3 = \frac{(1-x_2)(1-x_1)}{(1-x_3)} E_{\text{cm}}^2$$

and, therefore, it is required that

$$\frac{(1-x_1)(1-x_2)}{(1-x_3)} > \frac{8m_a^2}{E_{\text{cm}}^2}$$

for all m_q .

With these cutoffs there are more $q\bar{q}G$ - events in the Lund model than in the model by Hoyer et al. or in the model by Ali and Pietarinen³². In the Lund model there is no problem due to the difference since the excess events will be less two-jetty! As conclusions we note the following:

1. The Lund model produces more $q\bar{q}G$ events, but they are less three-jetty. The cutoffs in the matrix element should be carefully considered.
2. Strings provide a neat treatment of kinematics in the multijet final states and a transition from the 3-jet to 2-jet events.
3. The Lund model cannot be valid at higher energies (Ref. page 20).

JET AS A BRANCHING PROCESS

In the Leading Logarithm Approximation (LLA) of perturbative QCD an offshell parton is pictured as having a tree-like structure due to the multitude of decay processes that characterize its evolution in space and time (Fig. 21). The fragmentation function $D_a^b(z)$ (Eq. 1 page 5) now becomes a function of the maximal parton virtuality, i.e. $D_a^b(z) \rightarrow D_a^b(z, q^2)$. Within LLA only diagrams giving the maximum power of the

term $\alpha_s(\mu^2)\ln(Q^2/\mu^2)$ in each order, are summed. Parameter μ^2 characterizes the scale of the perturbative region and Q^2 the momentum transfer in the process. To get $D_a^b(z, Q^2)$ one sums up all possible "trees" and all possible final states (Fig. 21). This picture leads to a strong ordering of the parton energies and angles, i.e. $E_0 > E_1 > E_2 > \dots$, and $\theta_0 > \theta_1 > \theta_2 > \dots$.

The q^2 -evolution of the fragmentation functions may be expressed, within the LLA, in terms of the Altarelli-Parisi equations:

$$\frac{d}{dt} D_a^b(z, t) = \sum_c \int_z^1 \frac{dy}{y} \phi_a^c(y) D_c^b\left(\frac{z}{y}, t\right),$$

where t plays the role of the time variable

$$t(q^2, k^2) = \frac{1}{2\pi b} \ln \left(\frac{\alpha_s(k^2)}{\alpha_s(q^2)} \right) = \int_{k^2}^{q^2} \frac{dk^2}{k^2} \frac{\alpha_s(k^2)}{2\pi}$$

$$dt = \frac{\alpha_s(k^2)}{2\pi} \frac{dk^2}{k^2},$$

and $12\pi b = 11N_c - 2N_f$, $\alpha_s(q^2) = 1/b \ln(q^2/\Lambda^2)$. Function $\phi_a^c(z)$ is related to the decay probabilities $P_{ac}(z)$ by the relation

$$\phi_a^c(z) = P_{ac}(z) - \delta_{ac} \delta(1-z) \int_0^1 P_{ac}(y) dy,$$

where

$$P_{qq}(z) = P_{qG}(1-z) = C_q \frac{1+z^2}{1-z^2+\delta}$$

$$P_{Gq}(z) = \frac{1}{2} (z^2 + (1-z)^2)$$

$$P_{GG}(z) = C_G \left(\frac{1-z}{z} + \frac{z}{1-z+\delta} + z(1-z) \right)$$

with $C_q = (N_c^2 - 1)/2N_c$ and $C_G = N_c$; constant δ depends on the gauge.

In the Monte Carlo models for the parton showers one starts with calculating the probability for parton j not to decay down to $k^2 < q^2$, $\omega_j(q^2, k^2)$. The simplest possibility is to choose a fixed cutoff value and express the probability as

$$\omega_j(q^2, k^2) = e^{-\omega_j \cdot t(q^2, k^2)}$$

where ω_j is the overall probability per unit t for parton j to decay:

$$\omega_q = \int_{\epsilon}^{1-\epsilon} P_{qq}(z) dz$$

$$\omega_G = \int_{\epsilon}^{1-\epsilon} (P_{GG}(z) + N_F P_{Gq}(z)) dz.$$

The true kinematic limits for z , however, depend on the parton virtuality.

One may now proceed according to the following scenario:

(1^o) Sample invariant mass k_0^2 of the initial parton j_0 with energy q^2 according to the probability densities $\omega_j^N(q^2, k_0^2)$. Then generate the complete parton tree from j_0 .

(2^o) For each decay vertex $j \rightarrow j_1 + j_2$:

- If $j=G$ decide whether $j_1=G$ or $j_1=q$ using the weights ω_G^G, ω_G^q .
- Sample z from $P_{jj_1}(z)$ within the kinematical limits.
- Select the invariant masses $k_{j_1}^2, k_{j_2}^2$ according to $\omega_{j_1}^N, \omega_{j_2}^N$
- If $k_{j_1}^2, k_{j_2}^2 < (2\mu)^2$ set $k_{j_1}^2, k_{j_2}^2 = \mu^2$.
- Calculate transverse momentum between j_1, j_2 .
- Repeat the above procedure for the subsequent decays of $j_1, j_2 \dots$

until

$$k_{j_i}^2, k_{j_{i+1}}^2 \leq (2\mu)^2.$$

There are differences in the Monte Carlo models by different authors. For example, Odorico⁶ samples the masses k_i^2 at the beginning of each decay step and gets therefore slightly smaller parton transverse momenta than Kirschner and Ritter⁷. Also, Odorico uses the axial gauge.

When the complete parton trees have been generated the hadronization of the partons is carried out. Here one either resorts to the Field & Feynman jet algorithm or lets the transition region in space-time completely evaporate and then allows the partons to evolve to smaller masses ($O(m_p)$) and to decay within the allowed phase space restrictions.

RECIPES AND OBJECTIONS

We may conclude our discussion about the jet models with the following list of recipes:

1. Recipe of Hoyer et al. and Ali & Pietarinen (or the Lund model) assumes that only hard glue is important. If the mass of the quark-gluon system is smaller than some predetermined value ($O(3 \text{ GeV})$) the event is thrown out.
2. Recipe of Fox, Wolfram... , Odorico and Kirschner & Ritter: Generate parton showers with full off-shell kinematics. Evolve the showers until the size of the color singlet clusters reaches $\mu \gg \Lambda$. Then use the Field & Feynman jet algorithm to parameterize the transition region in space-time.
3. Recipe of Field, Fox, Wolfram: Transition region in space-time is completely evaporated: proceed as in recipe 2 but down to color singlet masses of the order $\sim m_p$. Then let the clusters 2-body decay using strings and phase space.
4. Recipe of the Lund group: The transition region is a flux tube stretched between the color charges (Fig. 18).

Objections to these recipes include:

1. This recipe cannot work at high energies, where $\sigma_{3\text{-jet}} > \sigma_0$,
2. There is an ambiguity between LLA and non-perturbative cluster parameterization, i.e. what is one testing with this recipe? There is also a question about applicability of the LLA itself, does it provide enough particles? The real tests of this recipe

are at higher energies.

3. This recipe has the same basic objections as 2 except the first point.
4. This recipe has the objections of 1. Cutoffs in the separation of 2 jet - 3 jet events seem to be somewhat ambiguous, too.

A TEST OF PERTURBATIVE QCD

A popular way to look for effects predicted by perturbative QCD is to evaluate moments of the inclusive distributions $D(z, Q^2)$ and study them as functions of Q^2 . The moment analyses frequently result in plots of the logarithm of one moment versus the logarithm of another moment³³. The slope measured from the plots is then, invariably, found to be in agreement with that predicted from ratios of anomalous dimensions γ_n in QCD; the basic QCD prediction reads for the moments $M_1(m, Q^2) = \int dx x^{m-1} F_1(x, Q^2)$,

$$M_1(m, Q^2) \approx -\gamma_n \ln(\ln(Q^2/\Lambda^2)) + \ln M_1^h,$$

and a plot of $\ln M(n, Q^2)$ versus $\ln M(n', Q^2)$ should result in a straight line. In Ref. 25 we have shown that a general form, assumed in a moment analysis, like

$$D^{NS}(z, Q^2) = C z^{f(Q^2)} (1-z)^\beta$$

where D^{NS} stands for a non-singlet fragmentation function, leads to straight lines in the log-log plots of moments of D^{NS} functions. Within fairly general constraints on the powers $f(Q^2)$ and β , the slope ratios $\gamma(n)/\gamma(n')$ fall in between the experimentally observed boundaries (Fig. 22).

The low energies available in current lepton-nucleon experiments introduce an effect that can be shown to account for the apparent scale violations in the moments of non-singlet fragmentation function³⁴. The non-singlet fragmentation functions in $(\nu)N$ interactions are defined as

$$D^{NS}(z, Q^2) = D^{h^+}(z, Q^2) - D^{h^-}(z, Q^2).$$

Integration over z gives us

$$\int D^{NS}(z, Q^2) dz \xrightarrow{Q^2 \rightarrow \infty} \langle Q_{jet} \rangle,$$

i.e. the zeroth moment is proportional to the electric charge of the jet. Our previous discussion (see page 15) shows that condition is valid only at the limit $W \rightarrow \infty$, i.e. $Q^2 \rightarrow \infty$ with x fixed. From our charge extrapolation results (page 15) we find the Q^2 -dependence of the moments

$$M(m, Q^2) \cong \int dz z^{m-1} D^{NS}(z, Q^2) \propto W^{-1}$$

due to the overlap between the target and current fragmentation regions. The $1/W$ dependence could be approximated by $1/Q$ dependence, but we may also use a direct parametrization of the net charge distribution through the overlap region in rapidity², i.e.

$$\Delta \propto \exp(-\lambda |\Delta Y^*|),$$

where $\Delta Y^* = |Y^* - Y_{max}^*|$, and λ is related to the correlation length in the central rapidity region. We thus get a general expression for the function $D^{NS}(z, Q^2)$ as

$$D^{NS}(z, Q^2) = C_e^{-\lambda |\Delta Y^*|} + C' z^\alpha (1-z)^\beta$$

where we choose the parameters α , and β to be $1/2$ and 3 , respectively, at the limit $Q^2 \rightarrow \infty$ and $\lambda = 1/2$. Using transformation $z \approx \frac{2m_T}{W} \sinh y^*$ we get an explicit parametrization of $D^{NS}(z, Q^2)$ with which we can calculate the moments $M(m, Q^2)$ by integrating numerically. Table 3 gives the slope ratios $\gamma(n)/\gamma(n')$ for our overlap based prediction, for the leading order QCD predictions and for the experimental values. The low energy effect is clearly able to explain the observed slope ratios. Leading order perturbative QCD does quite well, too. In Fig. 23 the moments $M(m, Q^2)$ are plotted for $x_{Bj} > 0.3$ as functions of Q^2 . The dashed lines represent our prediction that are based on the low energy overlap effect. As a conclusion we note that the moments of the fragmentation functions do not provide any decisive test of perturbative QCD. We also conclude that the so called double moment analyses³³ are likely to be even less decisive as tests of QCD³⁴.

x-DISTRIBUTIONS IN e^+e^- ANNIHILATION

In e^+e^- annihilation to hadrons no problems due to spectators exist but other mass effects are still present at low energies ($Q \leq 10$ GeV). In the following we shall study Q^2 -dependence of the $s(d\sigma/dx)$ distributions of hadrons in $e^+e^- \rightarrow$ hadrons; a way to demonstrate how the new quark thresholds effect x-distributions is to write the cross section $s d\sigma/dx$ explicitly down for different Q-regions, i.e.

$$s \frac{d\sigma}{dx} = \frac{\sum_i e_i^2 D_i(x, Q^2)}{\sum_i e_i^2}$$

(1°) Below charm threshold

$$s \frac{d\sigma}{dx} \approx D_u(x, Q^2)$$

(2°) Below beauty threshold

$$s \frac{d\sigma}{dx} \approx \frac{3}{5} D_u + \frac{2}{5} D_c$$

(3°) Below top threshold

$$s \frac{d\sigma}{dx} \approx \frac{6}{11} D_u + \frac{4}{11} D_c + \frac{1}{11} D_b$$

In Figs. 24 we plot the TASSO and MARKII data on $s \frac{d\sigma}{dx}$ for different c.m.s. energies³⁵. The dashed lines represent fits of the form $s \frac{d\sigma}{dx} = \sum_i \alpha_i x^{\alpha_i} (1-x)^{\beta_i}$ to the data. Comparing data at different $Q=\sqrt{s}$ we conclude that the distributions seems to be shifting towards smaller x-values as the c.m.s. energy increases. The shrinkage is expected when new heavy quark thresholds are crossed. The shrinkage is also a trademark of the perturbative QCD.

A simple way of looking into possible QCD effects is to concentrate on the large-x behaviour of the $s \frac{d\sigma}{dx}$ distributions¹¹. There the perturbative QCD prediction is particularly simple and we expect that the fragmentation function $D(x, Q^2)$ evaluated at $Q^2=Q_0^2$

$$D(x, Q_0^2) = A(1-x)^r$$

would be at $Q^2 > Q_0^2$ of the form¹¹

$$D(x, Q^2) = A \frac{\Gamma(r+1)}{x^{r+1} \Gamma(r+1+\xi(Q^2))} (1-x)^{r+\xi(Q^2)}$$

where $\xi(x, Q^2) = \frac{16}{3\beta_0} \log \left(\frac{\alpha_s(Q_0^2)}{\alpha_s(Q^2)} \right)$

and $\beta_0 = 11 - \frac{2}{3} N_f$, $\alpha_s(Q^2) = 4\pi / (\beta_0 \log(Q^2/\Lambda^2))$

In Fig. 25 we have plotted the exponent $\beta(Q^2) = r + \xi(Q^2)$ as a function of Q for two different x_{\min} selections, $x_{\min} > 0.2$ or $x_{\min} > 0.3$. The QCD prediction with $\Lambda = 400$ MeV is shown as the dashed line. We conclude that at low Q^2 -values the data exhibits more Q^2 dependence than predicted by the leading order perturbative QCD. This is quite natural considering mass effects present in this Q^2 region. A more complete analysis can be performed using the moments of the x -distribution i.e.

$$M(n, Q^2) = \int_0^1 dx x^{n-1} \left(s \frac{d\sigma}{dx} \right) .$$

In Fig. 26 we plot the moments $M(n, Q^2)$ for the recent TASSO and MARK II data using the fits shown in Fig. 24. The dashed lines represent leading order perturbative QCD predictions with $\Lambda = 400$ GeV. The predictions seem to fit the data for low n ($n \leq 3$) but clearly underestimate the Q^2 -dependence of the higher moments at low Q^2 -values. In the log-log plot the straight lines are produced³⁶!

Conclusions

Jets mean different things for different people: a quark combining with quark-antiquark pairs in the chromomagnetic field, a tree-like parton shower, a limited transverse momentum spray of hadrons, a shower of hadrons contained in an angular cone, a cluster of hadrons in the momentum space, a consequence of constraints imposed by the transversely limited phase space... For some individuals there are no jets and for some others jets are a quest for a life long dedicated search.

We may study properties of quark jets in the e^+e^- annihilation to hadrons or in the deeply inelastic lepton-nucleon collisions at the presently available energies. In hadron-hadron collisions inclusive jet production can not be studied due to the small hard scattering cross sections and different kinds of "jets" are defined by the triggering schemes available for the experiments. With the help of the detailed information deduced from e^+e^- and pN collisions predictions for the event shapes in hadron-hadron collisions can be made. The model by Field, Fox, Wolfram etc. for the parton showers can be used in qualitative comparisons of the observed event configurations. The model also provides means for more "realistic" acceptance calculations in a high energy experiment. In general, we should forget the hunt of individual "jets" in hadronic collisions and concentrate in the details of confinement: how do the multiparton states convert into the observed hadrons? Here, one should keep in mind that we have only touched the surface of the jet phenomena; complications due to coherent phenomena have been ignored in our discussion.

Recently, a class of analyses that are based on moments of inclusive particle distributions in lepton-nucleon collisions has become popular as a test of perturbative QCD. In Part I of this talk we have pointed out serious problems in the interpretation of these results. The phase space limitations at energies below 10 GeV do not allow unambiguous conclusions from these tests. The potential of the x -distributions in e^+e^- annihilation to hadrons as a test of perturbative QCD is introduced and it is shown that, similarly to the nucleon structure functions, no definite evidence for the perturbative QCD effects can be established.

I want to express my gratitude to the organizers of this excellent and realistic workshop. I am also grateful to Marti Bennett and Carmen Vera at Fermilab for the typing and drawings in this article.

REFERENCES:

1. Observations by Fairbanks are here ignored.
2. See for example, R. Orava, *Physica Scripta*, 25 (1982) 159.
3. R.D. Field and R.P. Feynman, *Nucl. Phys.* B136 (1978) 1.
4. S.D. Ellis, *Jets and Quantum Chromodynamics*, Lectures given at the NATO Advanced Study Institute in Elementary Particles, July 9-12, 1979, Boulder, Colorado, USA.
5. G. Fox, *Untangling jets from hadronic final states*, CALT-68-863 (1981), and references cited therein.
6. R. Odorico, *Exclusive calculations for QCD jets in a Monte Carlo approach*, ECFA-LEP Note SSG/8/9 (1980) and University of Bologna preprint IFUB 80/5 (1980).
7. S. Ritter, *QCD jets in e^+e^- annihilation and their transition into hadrons*, Karl-Marx University preprint KMU-HEP 82-03 (1982), and references cited therein.
8. K. Konishi, A. Ukawa and G. Veneziano, *Phys. Lett.* 78B (1978) 243 and *Phys. Lett.* 80B (1979) 259.
9. G. Sherman, S. Weinberg, *Phys. Rev. Lett.* 39 (1977) 1436.
E. Fahri, *Phys. Rev. Lett.* 39 (1977) 1587.
H. Georgi and M. Machaek, *Phys. Rev. Lett.* (1977) 1237.
C.L. Basham, L.S. Brown, S.D. Ellis and S.T. Love, *Phys. Rev.* D17 (1978) 2298.
S. Brandt and H. Dahmen, *Z. Phys.* C1 (1979) 61.
G.C. Fox and S. Wolfram, *Nucl. Phys.* B149 (1979) 413.
A. Duncan, S. Gupta and A. F. Mueller, *Nucl. Phys.* B175 (1980) 148.
10. T. Sjostrand, *The Lund Monte Carlo for jet fragmentation*, University of Lund preprint LU TP 82-3 (1982) and references cited therein.
11. R.D. Field, *The production of partons and hadrons in e^+e^- annihilations - quark and gluon jet models*, Invited talk presented at the conference on Perturbative QCD held at Florida State University, Tallahassee, March 26-30, 1981, University of Florida preprint UFTP 81-12 (1981) and references cited therein.
R.D. Field and S. Wolfram *QCD model for e^+e^- annihilations*, U. of Florida preprint UFTP-82-12 (1982).
12. R.D. Field, G.C. Fox and R.L. Kelly, *Gluon bremsstrahlung effects in hadron-hadron collisions*, U. of Florida preprint UFTP-26-82 (1982) and references cited therein.
13. J.D. Bjorken, "Current Induced Reactions", Lecture notes in *Physics* 56, Ed. J.G. Korner et al. (Springer-Verlog, 1976) 93.
J.D. Bjorken, *QCD and the space-time evolution of high energy e^+e^- , pp, and heavy ion collisions*, Fermilab-Conf-82/42-THY (1982), presented at the 2nd International Conference on "Physics in Collision", Stockholm, Sweden, 2-4 June, 1982.
14. S.J. Brodsky and N. Weiss, *Phys. Rev.* D16 (1977) 2325.
15. P.K. Malhotra and R. Orava, *Measurement of Strange Quark Suppression in Hadronic Vacuum*, Fermilab-Pub-82/79 (1982).
16. R. Migneron et al., *Production of protons and lambdas in e^+e^- jets from jet calculus and the recombination model*, Fermilab-Pub-82/15-THY (1982) and SLAC-Pub-2861 (1982) and references cited therein.

17. K.W. Bell et al., A survey of models of baryon production in e^+e^- annihilation, Rutherford preprint RL-82-011 (1981).
An excellent review can be found from: V.P. Sukhatme, Invited Review Talk at the XIII International Symposium on Multiparticle Dynamics, Volendam, The Netherlands, June 1982.
18. V.V. Amosov et al., Phys. Lett. 93B (1980) 210.
19. J. Bell et al., Phys. Rev. D19 (1979) 1.
20. W.G. Scott in the proceedings of the Neutrino-78 Conference, Purdue University, 1978, Ed. by E.C. Fowler.
21. J.P. Berge et al., Nucl. Phys. B184 (1981) 13.
22. H.F. Daum, H. Meyer and J. Burger, A cluster algorithm for jet studies, DESY 80/101 (1980).
V. Hepp, Talk given at the XXth International Conference on High Energy Physics, University of Wisconsin, Madison, 1980.
23. J.J. Aubert et al., CERN-EP/82-47 (1982), to be published in Phys. Lett. B.
24. A. Krzywicki and D. Weingarten, Phys. Lett. 50B (1974) 265.
25. R. Orava, Structure of Quark jets, Invited talk in the VII International Symposium on Multiparticle Dynamics, Notre Dame, Indiana, 21-26 June, 1981, Ed. by W.D. Shepard and V.P. Kenney (1982).
26. R. Orava, Phys. Rev. D24 (1981) 1424.
27. G.R. Farrar and J.L. Rosner, Phys. Rev. D7 (1973) 2747.
28. J.P. Berge et al., Phys. Lett. 91B (1980) 311.
J.P. Berge et al., Nucl. Phys. B184 (1981) 13.
29. R. Erickson et al., Phys. Rev. Lett. 42 (1979) 822.
30. D. Amati, The structure of hard processes from QCD, CERN preprint TH.2650-CERN (1979).
31. P. Hoyer et al., Nucl. Phys. B161 (1979) 349.
32. A. Ali et al., Phys. Lett. 93B (1980) 155.
33. J. Blietschau et al., Phys. Lett. 87B (1979) 281.
P. Allen et al., Nucl. Phys. B176 (1980) 333.
H. Deden et al., Nucl. Phys. B198 (1982) 365.
34. R. Orava and K. Lassila, Magic of the Moments - Re-examination of Q^2 dependence in fragmentation functions, to be published.
35. J.F. Patrick et al., SLAC-PUB-2936 (1982)
R. Braudelik et al., Phys. Lett. 114B (1982) 65.
D. Schlatter, private communication (1982).
36. D. Jaffe, A. Ng, R. Orava and K. Lassila, to be published.

Table 1. Probabilities P_i

Process	P_i
$e^+e^- \rightarrow \text{hadrons}$	$\frac{e_i^2}{\sum_i e_i^2}$
$eN \rightarrow e+\text{hadrons}$ $\mu N \rightarrow \mu+\text{hadrons}$	$\frac{\left\{ (1-y)^2 + 1 \right\} e_i^2 x f_N^{q_i}(x)}{\sum_i e_i^2 x f_N^{q_i}(x)}$
$\nu N \rightarrow \mu + \text{hadrons}$	$\frac{x \left\{ f_P^{q_i}(x) + (1-y)^2 f_P^{\bar{q}_i}(x) \right\}}{\sum_i x \left\{ f_P^{q_i}(x) + (1-y)^2 f_P^{\bar{q}_i}(x) \right\}}$
$\bar{\nu} N \rightarrow \mu + \text{hadrons}$	$\frac{x \left\{ f_P^{\bar{q}_i}(x) + (1-y)^2 f_P^{q_i}(x) \right\}}{\sum_i x \left\{ f_P^{\bar{q}_i}(x) + (1-y)^2 f_P^{q_i}(x) \right\}}$
$AB \rightarrow \gamma + X$ $\downarrow q_i \bar{q}_i$	$\frac{e_i^2 x_a x_b \left\{ f_A^{q_i}(x_a) f_B^{\bar{q}_i}(x_b) + f_A^{\bar{q}_i}(x_a) f_B^{q_i}(x_b) \right\}}{\sum_i e_i^2 \left\{ f_A^{q_i}(x_a) f_B^{\bar{q}_i}(x_b) + f_A^{\bar{q}_i}(x_a) f_B^{q_i}(x_b) \right\}}$

$f(x)$ is the parton momentum density distribution within the nucleon.

Table 2.

HIERARCHY OF MODELS

MODEL	QCD	BARYONS	HEAVY QUARKS	DI-QUARKS
Field & Feynman	-	-	-	-
Hoyer	$O(\alpha_s)$	-	YES	-
Alli & Pietarinen	$O(\alpha_s^2)$	-	YES	-
LUND	$O(\alpha_s^2)$	YES	YES	YES
Fox & Wolfram	LLA			
Odorico	LLA			
Kirschner & Ritter	LLA			
KUV Jet Calculus + Recomb.	LLA	YES	YES	-

Table 3: Slope ratios

$\gamma(n')/\gamma(n)$	OVERLAP	QCD	EXP
$\gamma(6)/\gamma(4)$	1.26	1.29	$1.27 \pm .10$
$\gamma(7)/\gamma(3)$	1.86	1.76	$1.67 \pm .17$

FIGURE CAPTIONS

- Fig. 1. Space-time picture of jet formation in a hard scattering process¹³.
- Fig. 2. Hard scattering process in (a) $e^+e^- \rightarrow \text{hadrons}$, (b) $\ell N \rightarrow \ell + \text{hadrons}$, and (c) $hh \rightarrow \text{hadrons}$.
- Fig. 3. Illustrations of expected rapidity distributions (a) for $e^+e^- \rightarrow \text{hadrons}$, (b) for deeply inelastic interactions $\ell N \rightarrow \ell + \text{hadrons}$, and (c) for qq -annihilation to hadrons in deeply inelastic hadron-hadron collisions.
- Fig. 4. Fractional energy distributions $D(z) \approx 1/N_{ev} \frac{dN}{dz}$ for hadrons produced in e^+e^- -annihilation and in deeply inelastic ℓN collisions. The solid line is the Field & Feynman jet parametrization².
- Fig. 5. Fractional energy distributions $D(z) \approx 1/N_{ev} \frac{dN}{dz}$ for hadrons produced in e^+e^- -annihilation and in deeply inelastic ℓN collisions. The solid and dashed lines represent the Field & Feynman jet parametrization²⁰ and the "uncorrelated" LPS prediction²⁰.
- Fig. 6. An illustration of the Limited p_T Jets.
- Fig. 7. An illustration of the Angular Jets.
- Fig. 8. Distribution of the angle between the two most collinear particles in the Field & Feynman Jets²².
- Fig. 9. Test of the Cluster Jet algorithm with the PLUTO data (solid circles) with Monte Carlo generated qq -events (Δ) and qqg -events (\square)²².
- Fig. 10. Factorization test with data from an νN experiment at Fermilab. The ratio $R = D(z_1, x_1) / D(z_1, x_2)$ is plotted as a function of z for different fixed Q^2 values².

- Fig. 11. Factorization test by the European Muon Collaboration²³.
- Fig. 12. Definition of the rapidity zones.
- Fig. 13. Distributions of rapidity zone lengths for two different definitions: (1^o) for forward zone zones only, and (2^o) for zones with one zone overlapping with the target fragmentation region²⁶.
- Fig. 14. The average zone length as a function of the c.m.s. energy for two different zone definitions. The two data points represent pp data. The dashed line is obtained by randomly reassigning the electric charges of final state particles²⁶.
- Fig. 15. Average net charge of the hadrons traveling forward (in the current direction) in the hadronic c.m.s. in $(\nu)N$ charged current interactions as a function of $1/W$. An "uncorrelated" Monte Carlo prediction is shown as the shaded area².
- Fig. 16 Strange quark suppression factor $\lambda_{ss/uu}$ as a function of the available energy in different processes¹⁵.
- Fig. 17. Illustration of the use of the strings in the definition of 3-jet and 2-jet events.
- Fig. 18. Illustration of the branching process in the LLA of perturbative QCD.
- Fig. 19. Illustration of the space-time evolution of a hard scattering final state with one hard gluon emission¹³.
- Fig. 20. Illustration of the space-time evolution of a hard scattering final state at very high energy with several gluon emissions - a branching process.
- Fig. 21. Illustration of the branching process in LLA of perturbative QCD.
- Fig. 22. Slope ratios $\gamma(7)/\gamma(3)$ and $\gamma(6)/\gamma(4)$ for the logarithms of the non-singlet moments of the quark fragmentation functions as functions of parameters β and f (see the text)^{25,34}.

Fig. 23. Non-singlet moments of quark fragmentation functions as functions of Q^2 for νp data at $x_{Bj} > 0.3$. The dashed lines represent our predictions that are based on the kinematical overlap³⁴.

Fig. 24. MARK II (PEP) and TASSO (PETRA) data for $s \, d\sigma/dx$ with different fixed \sqrt{s} values³⁵. The dashed lines represent our parameterisations.

Fig. 25. Exponent β in $s(d\sigma/dx)^{x > x_0} = (1-x)^\beta$ as a function of Q for different x_0 -values= $x_0=0.2$ and $x_0=0.3$ for the TASSO and MARK II data.

Fig. 26. Moments of the $s(d\sigma/dx)$ distributions as functions of Q^2 for the MARK II and TASSO data³⁶.

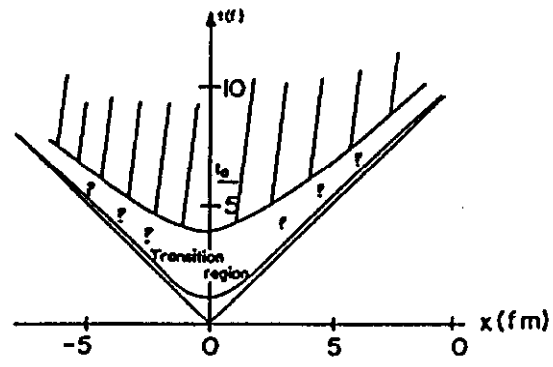


Fig. 1

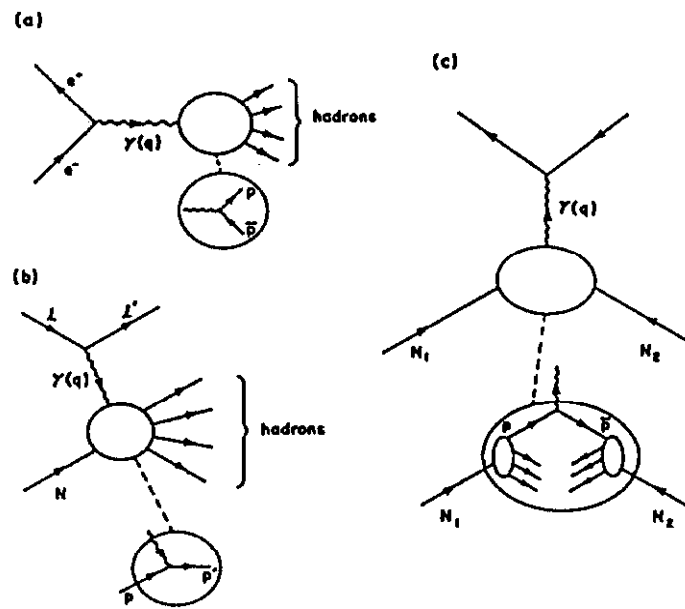


Fig. 2

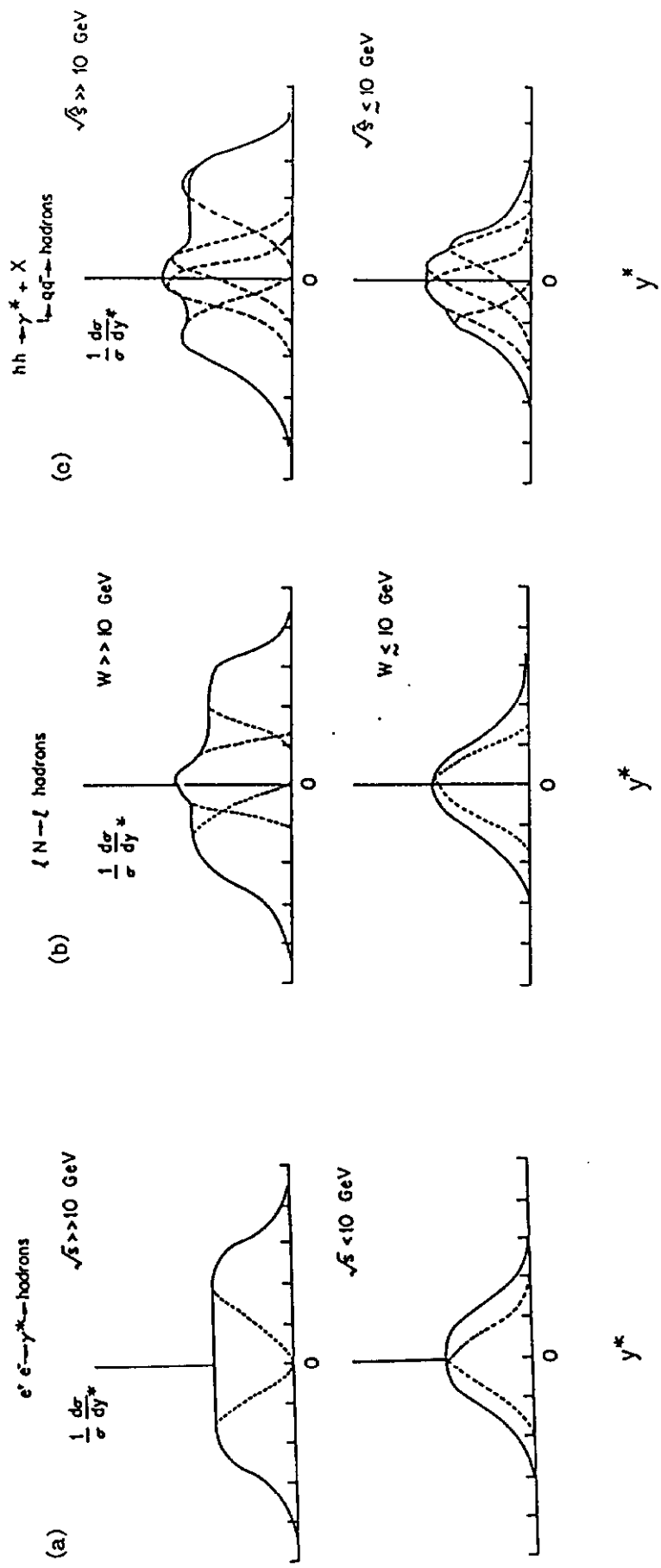


Fig. 3

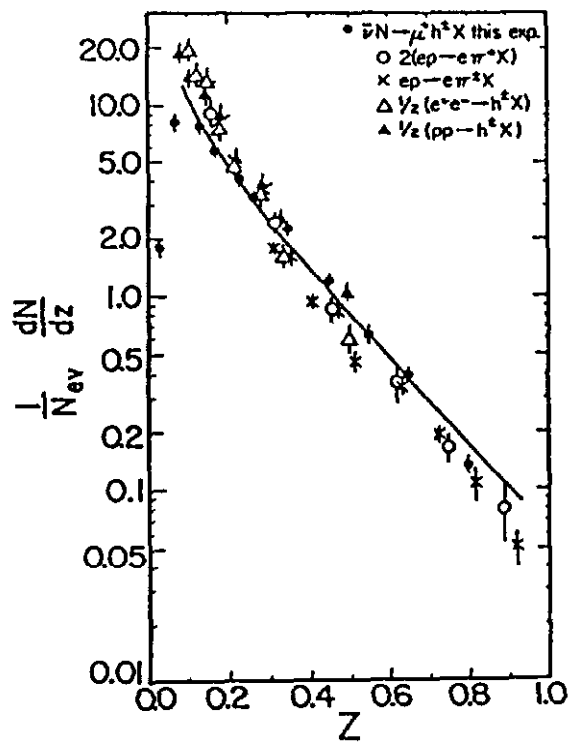


Fig. 4

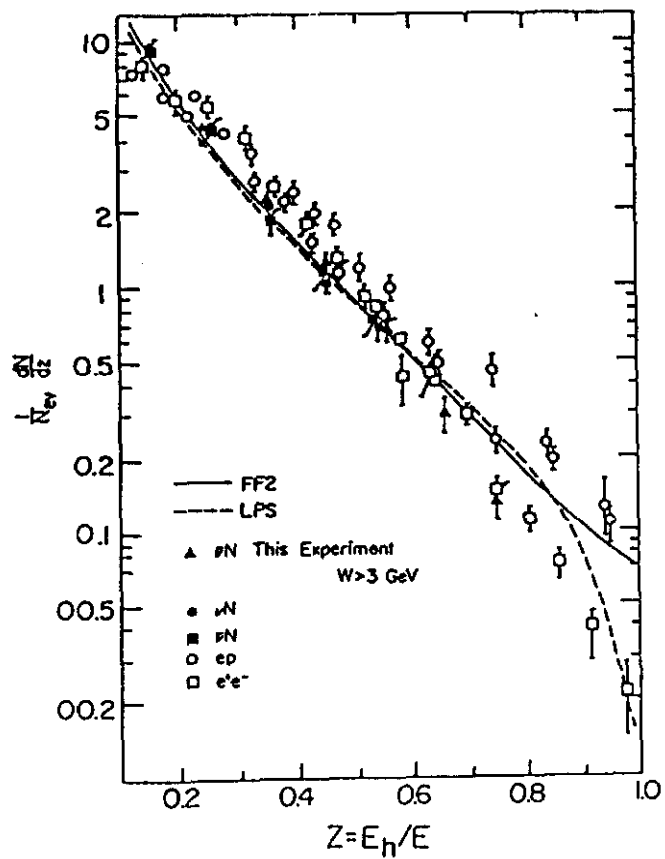


Fig. 5.

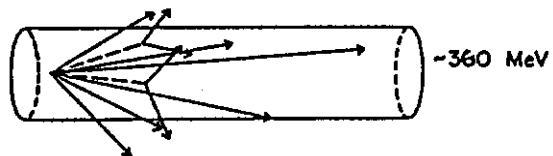
LIMITED P_T JET

Fig. 6

ANGULAR JET

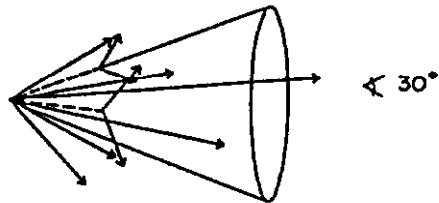


Fig. 7

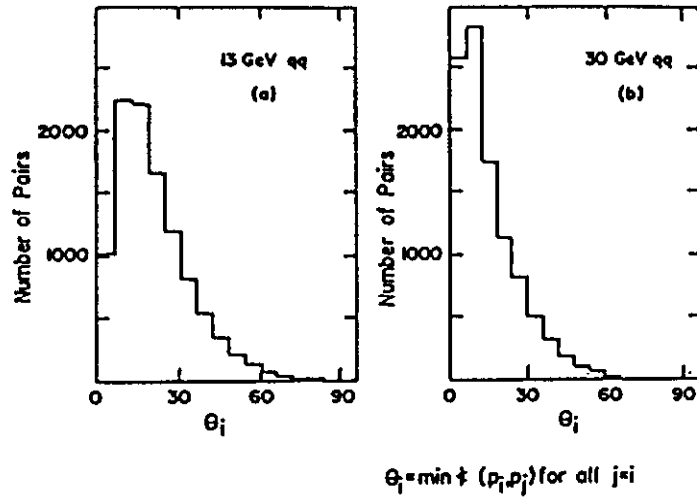


Fig. 8

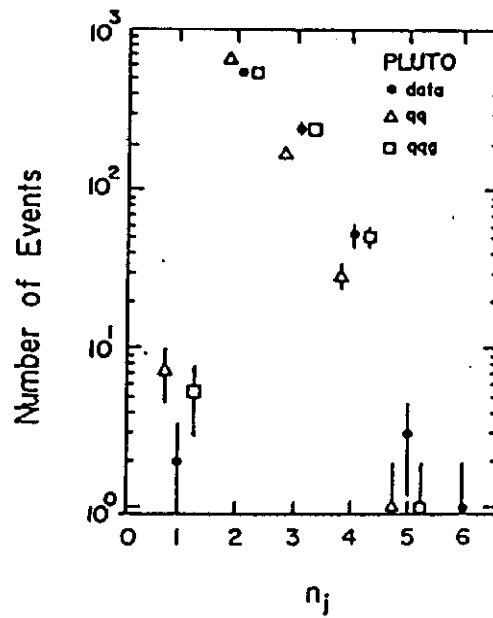


Fig. 9

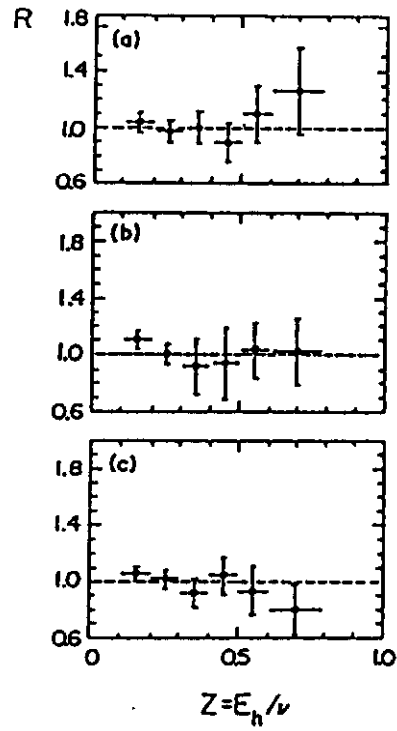


Fig. 10

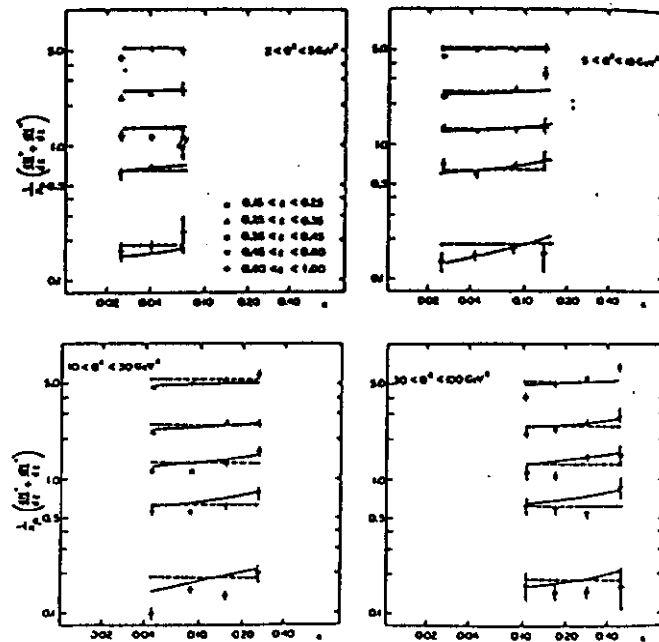


Fig. 11

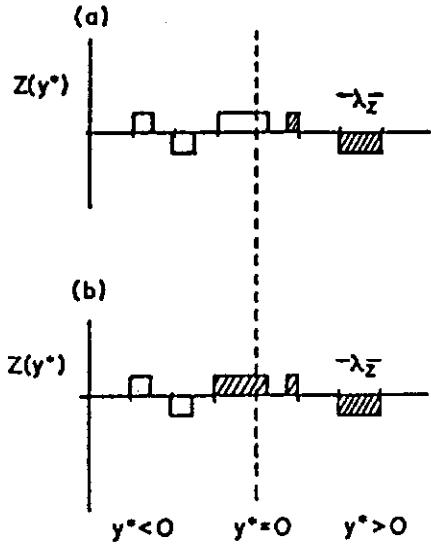


Fig. 12

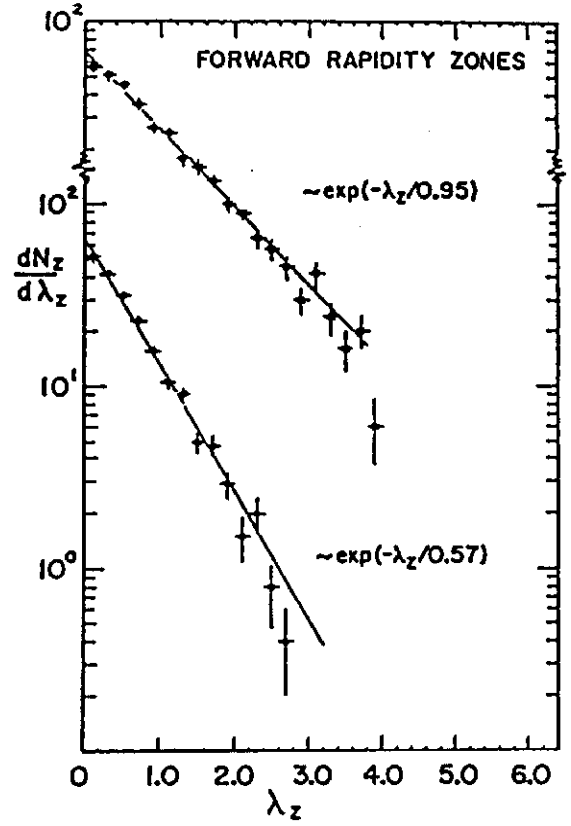


Fig. 13

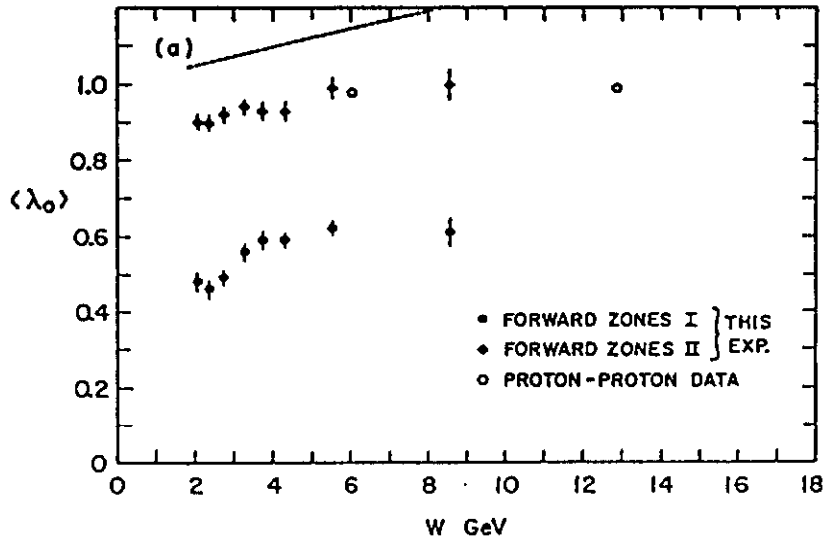


Fig.14

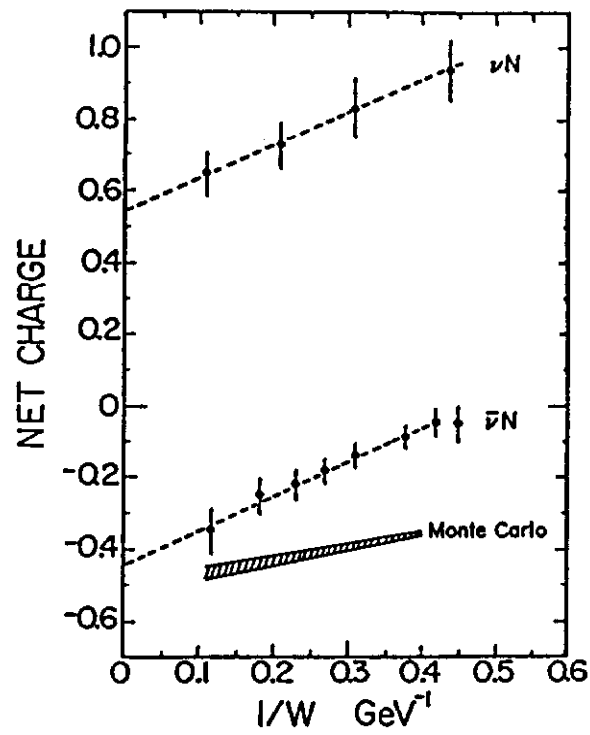


Fig. 15

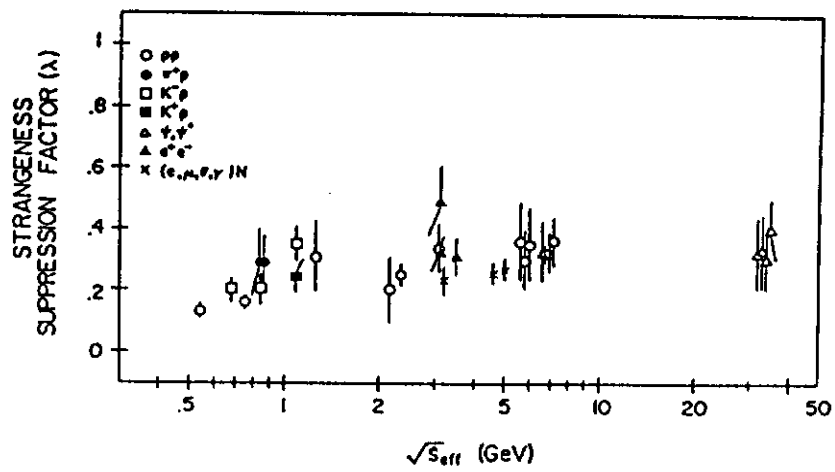


Fig. 16

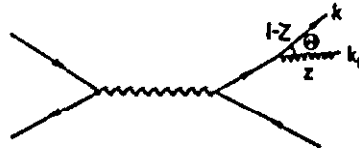


Fig. 17

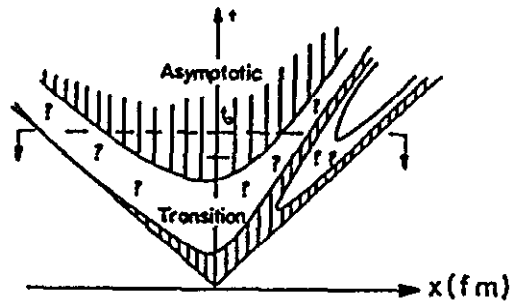


Fig. 18

Y

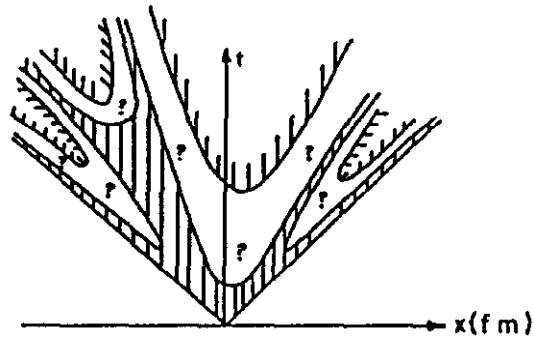


Fig. 19

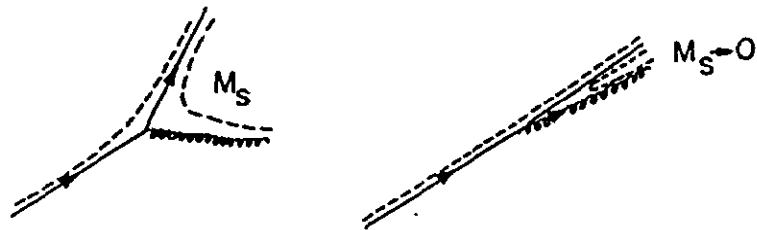


Fig. 20

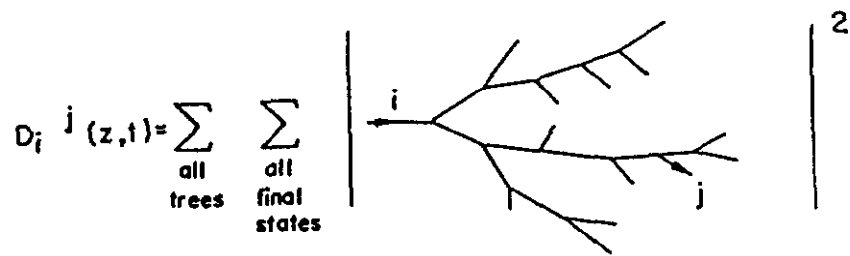


Fig. 21

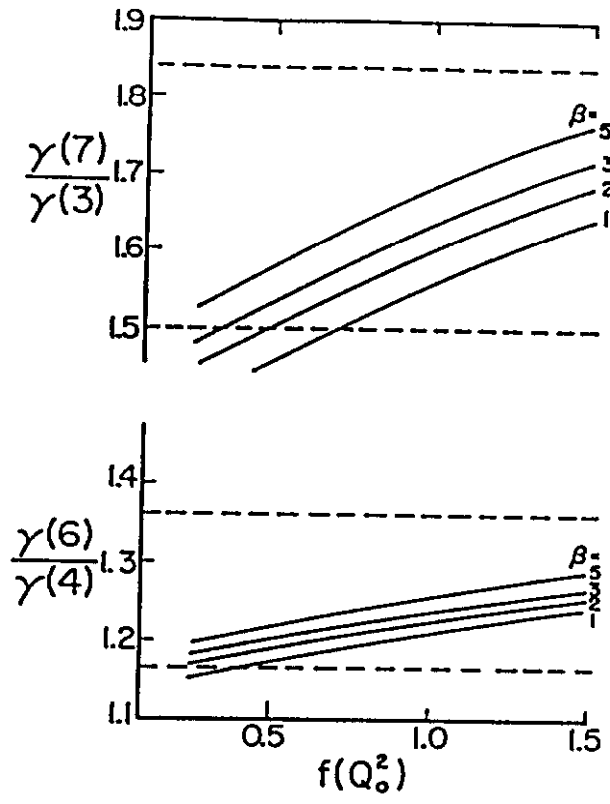


Fig. 22

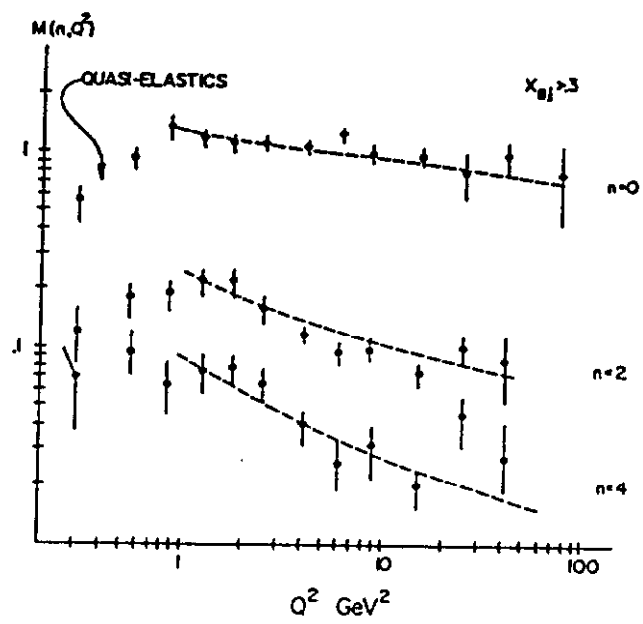


Fig. 23

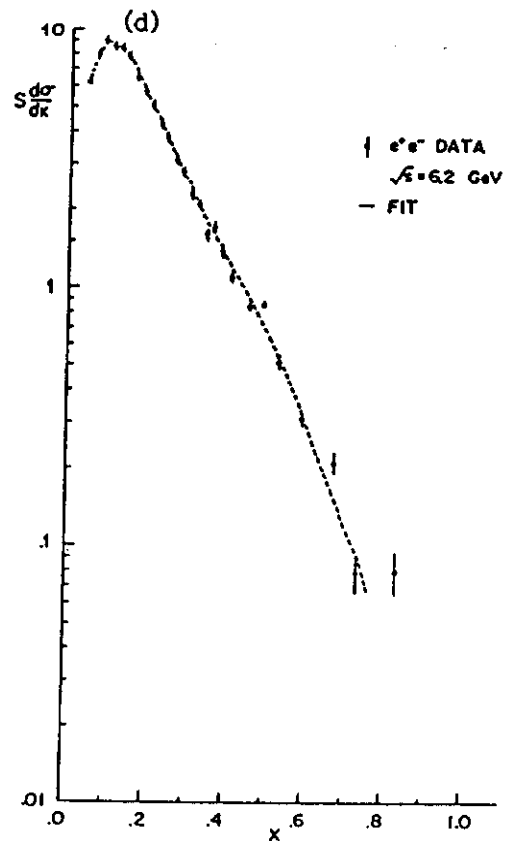
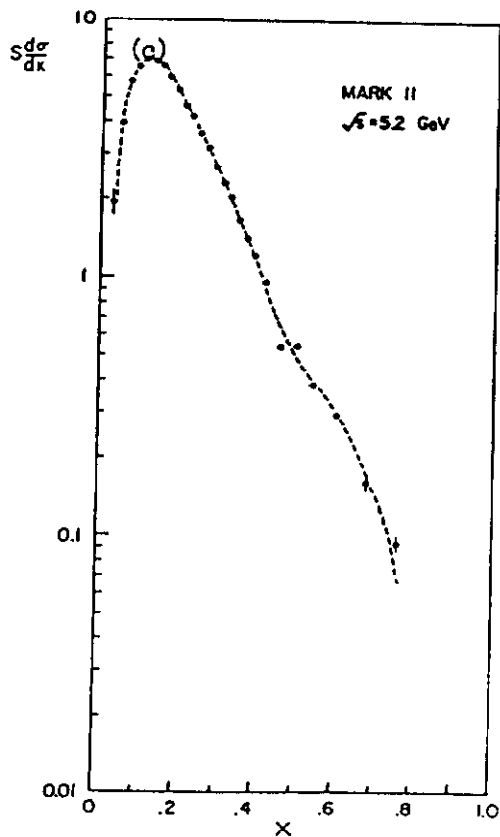
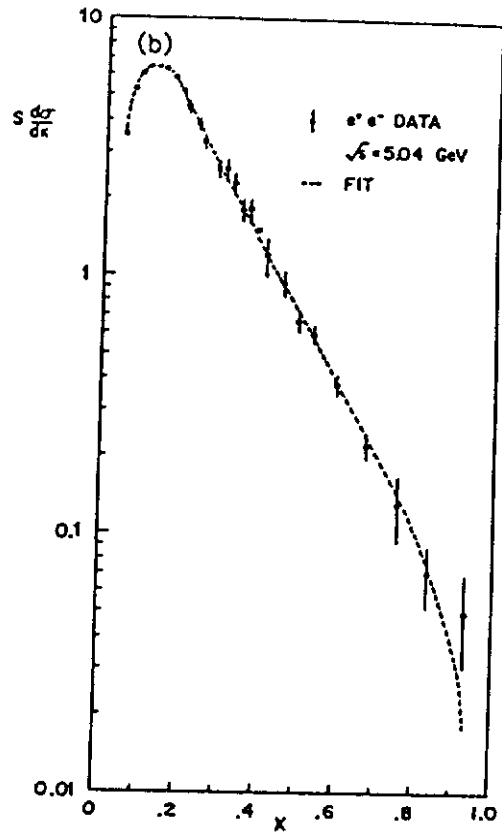
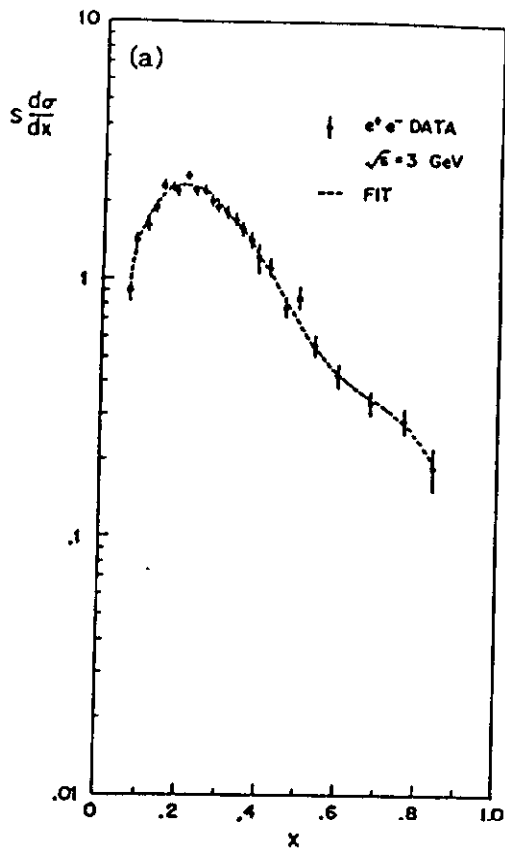


Fig. 24

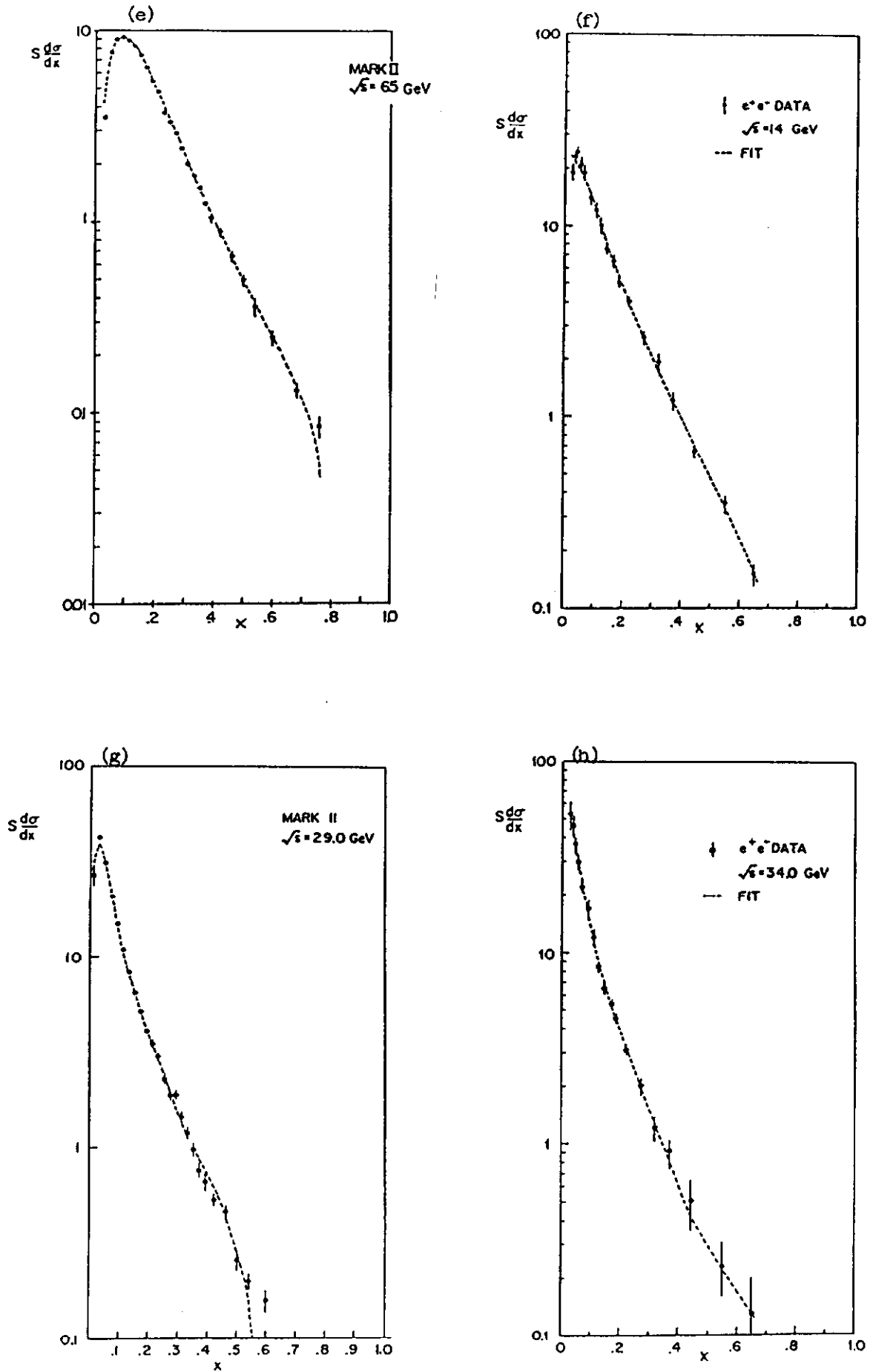


Fig. 24

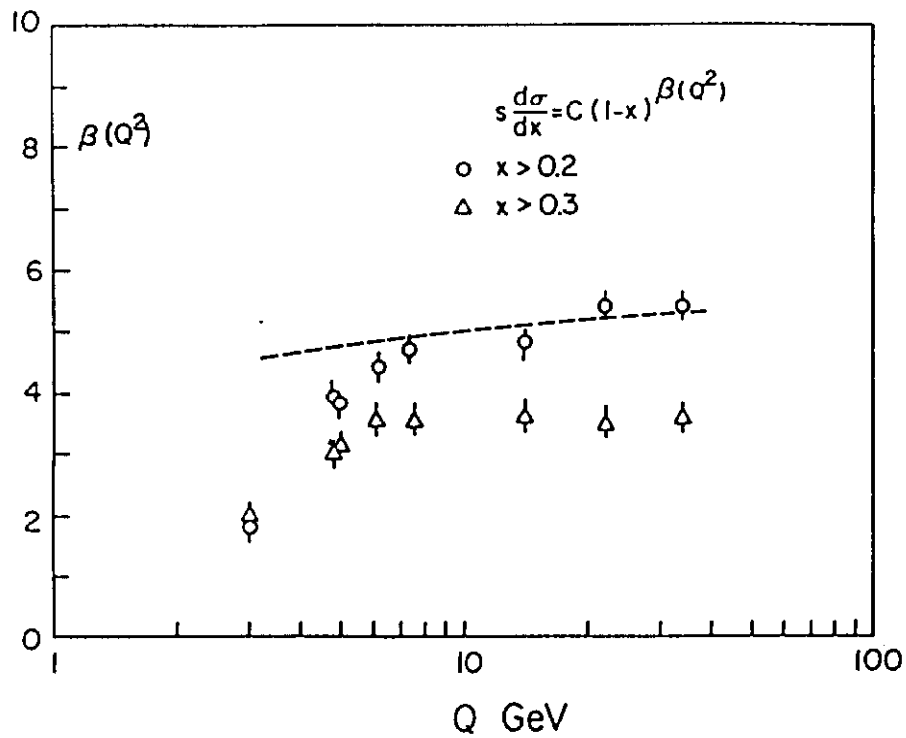


Fig. 25

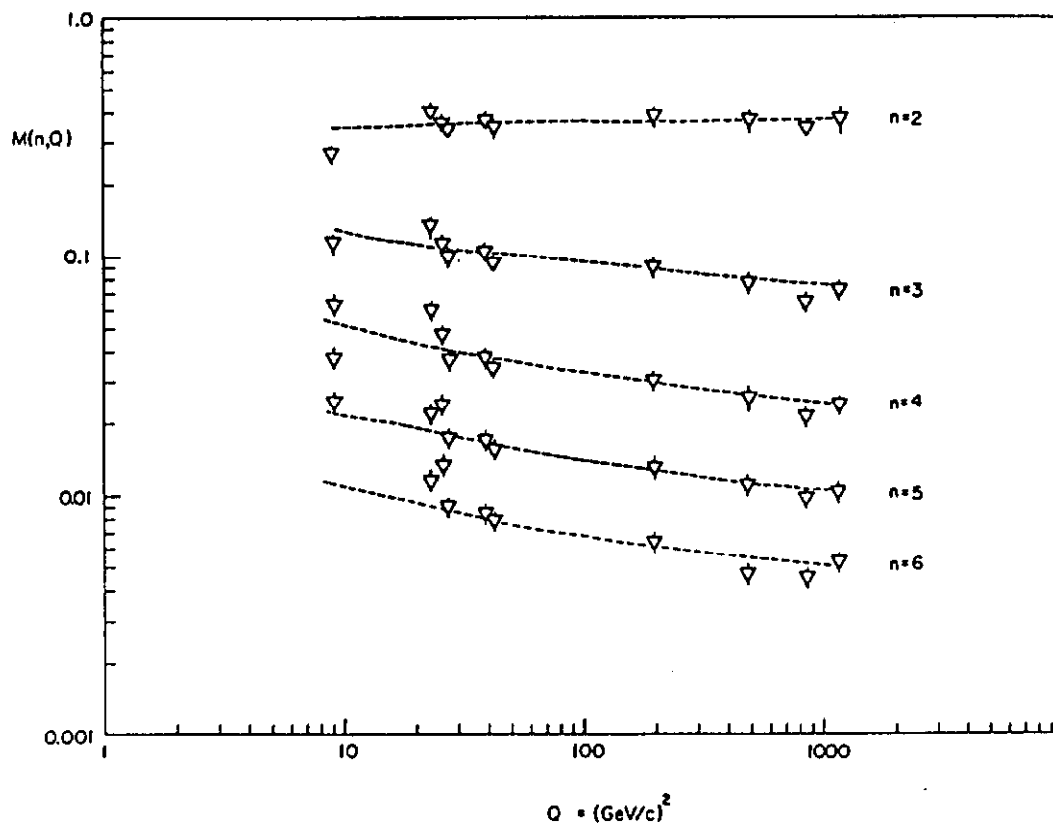


Fig. 26